

Chapter 4

BEAM OPTICS

4.1 Introduction

Since the usefulness of the synchrotron radiation source is connected to its satisfying to the experimental demands by offering the needed photon energy and brilliance, the scientific case of SESAME was upgraded due to the recent demands for higher photon energies with high brilliance.

Going with the machine energy from 2 GeV to 2.5 GeV was the convenient solution for this requirement.

$$\epsilon_c \text{ (keV)} = 0.665 B(T) E^2 \text{ (GeV)} \quad (4.1)$$

This needed changes in some parameters of the last version and modifications in its characteristics [1].

The low emittance is the most efficient solution to get high brilliance. Since the emittance increases with the square of the machine energy,

$$\epsilon_x = C_q \gamma^2 \langle H \rangle_{\text{mag}} / J_x \rho \quad (4.2)$$

Where:

$$\langle H \rangle_{\text{mag}} = \int (\gamma_x \eta^2 + 2\alpha_x \eta \eta' + \beta_x \eta'^2) ds / 2\pi\rho \quad (4.3)$$

$$J_x = 1 - I_4 / I_2, \quad I_4 = \int_{\text{BM}} (1 - 2n) \eta ds / \rho^2, \quad I_2 = \int_{\text{BM}} 1 ds / \rho^2, \quad C_q = 3.84 \cdot 10^{-13} \text{ mrad}$$

Efforts should be done to minimise it by using another optical aspects and designing strategies.

The SESAME storage ring lattice had to go through some modifications taking into account the different geometrical, financial and optical restrictions that made these modifications to be challenging.

4.2 The Lattice

4.2.1 The Unit Cell

An increase in the machine energy from 2 to 2.5 GeV with keeping the bending magnets (BMs) enough below the saturation limit, resulted in an increase in the curvature radius (ρ) of the BM according to equation (4.4):

$$B(T)\rho(m) = E(\text{GeV})/0.2998 \quad (4.4)$$

The resulted curvature radius was 5.9565 m, together with a little increase in the field flux in the BMs to 1.4 T. This in turn increased the length of the BM to 2.34 m.

The high-energy radiation with high brilliance from the insertion devices has a priority in SESAME case. So, a special care was given to offering an enough number of straight sections with reasonable lengths to accommodate the different insertion devices, and getting as low emittance as possible.

The storage ring circumference was limited by geometrical restrictions which put a limit to the idea of increasing the curvature radius (ρ) to decrease the emittance (see equations (4.2) and (4.3)). The better idea was to increase the horizontal damping partition number (J_x) by increasing the field gradient in the BMs to 3.032 (T/m), and decreasing the dispersion in the BMs (η) by increasing the dispersion in the straight sections.

The idea of using BMs with gradient which can be varied by $\pm 6\%$ was consumed to eliminate the vertically-focusing quadrupoles and keep just the horizontally-focusing ones in 2 families. By this step, more spaces between the magnetic elements have been gained, longer sections for the insertion devices have been offered and the number of used quadrupoles has been reduced. Figure (4.1) shows the difference in the cell structure between the previous ring lattice (in the white book) and the new upgraded one.

Reducing the machine flexibility was the most considerable disadvantage of this step, but it will be shown that this will not have a significant impact on the machine performance except that it confines us to a limited freedom in changing the integer vertical tune which calls for a special care in choosing the working point.

Keeping the sextupoles in 4 families was necessary for non linear optimisations and compensations for the effect of insertion devices on the dynamic aperture and tune shift with amplitudes. This flexibility is necessary to get a large dynamic aperture, especially that the chromaticity will be corrected, at least, to 2 in both planes.

The upgraded SESAME storage ring lattice with its optical functions is shown in figure (4.2), and its structure elements are given by table (4.1). Attention should be paid here to the fact that the strength of the sextupole (m) in the table is defined by $(1/2B\rho)\partial^2B_z/\partial x^2$.

The ratio (\sum straight section length/circumference) is a figure of merit for storage ring compactness. The upgraded SESAME lattice occupies a high level in this criteria among the synchrotron radiation sources in the world. SESAME storage ring parameters are given in table (4.2).

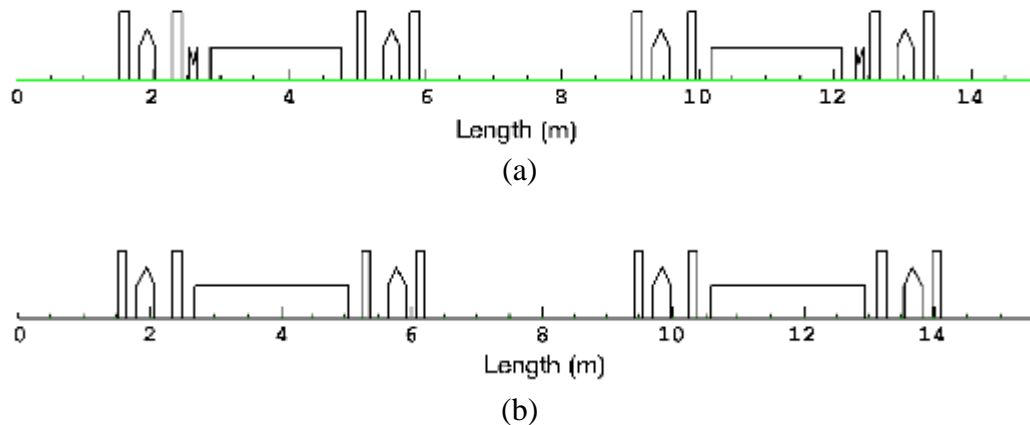


Figure 4.1: The structure of one super period (2cells) of: (a) the white book lattice and (b) the upgraded lattice (in this yellow book).

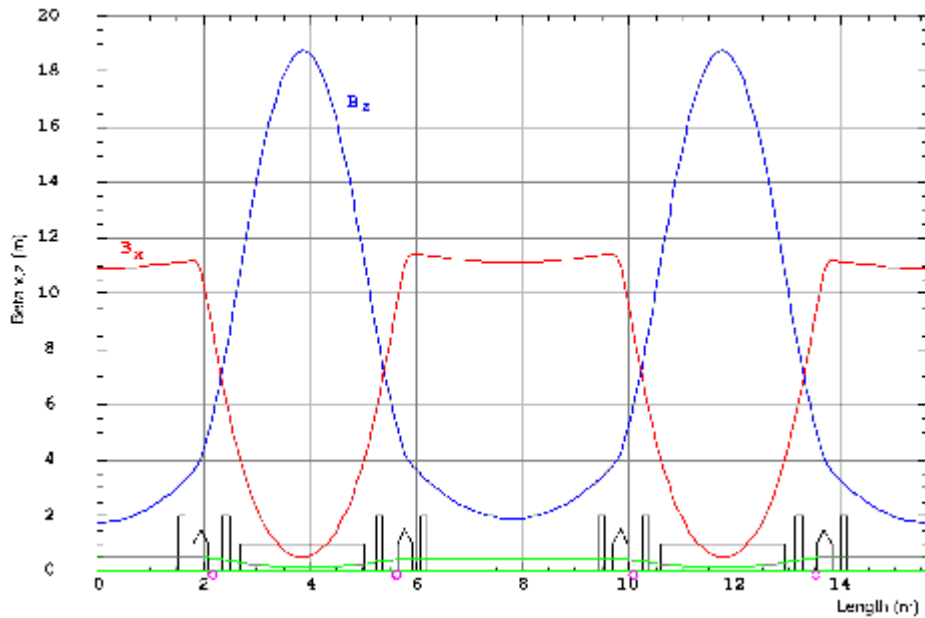


Figure 4.2: Optical functions of SESAME lattice, the green line represents dispersion. The pink circles represent bPMs.

A resulted relatively high β_z in the BMs accompanied by a high decoupling between the vertical and horizontal betatron functions was consumed to increase the bending gradient efficiency in changing the vertical tune and compensating for the tune shift and beta beating caused by the insertion devices. On the other hand a high care should be taken in aligning the BMs during the installation process.

It should be mentioned here that the above optics is the “bare lattice optics” i.e. without insertion devices. The optimum optics for several cases of insertion devices has been investigated (see section 4.3).

**Table 4.1: The lattice elements of half-super period structure.
The total ring is 8 super periods.**

Name code	Element	Length(m)	$\rho(m)$	$k(m^{-2})$	$m(m^{-3})$
1	D1	1.505			
2	SI	0.14			9.1941
3	D2	0.155			
4	Q1	0.285		2.038	
5	D3	0.255			
6	S2	0.14			-12.9194
7	D4	0.205			
8	BM	2.34	5.95651	-.36358	
9	D5	0.205			
10	S3	0.14			-12.5963
11	D6	0.255			
12	Q2	0.285		2.02928	
13	D7	0.155			
14	S4	0.14			8.94741
15	D8	1.596			

**Table 4.2: SESAME storage ring parameters
(without insertion devices).**

Parameter	Unit	Value
General Parameters		
Energy	GeV	2.5
Maximum Beam current	mA	400
Circumference	m	124.802
Natural emittance	nm.rad	24.9
Coupling	%	1
Horizontal emittance	nm.rad	24.65
Vertical emittance	nm.rad	0.2465
Horizontal tune		7.217
Vertical tune		5.192
Relative energy spread	%	0.1119
Chromaticity (horizontal)		-13.1
Chromaticity (vertical)		-13.8
Machine Functions		
Horizontal beta functions		
Wiggler / bending / undulator	m/rad	11.12 / 0.483 / 10.9
Vertical beta functions		
Wiggler / bending / undulator	m/rad	1.89 / 18.75 / 1.73
Dispersion function		
Wiggler / bending / undulator	m	0.453 / 0.135 / 0.534
Beam Sizes and Cross Sections		
Horizontal beam size		
Wiggler / bending /undulator	μm	728.6 / 186.3 / 790.9
Vertical beam size		
Wiggler / bending / undulator	μm	21.6 / 68 / 20.6
Beam area		
Wiggler / bending / undulator	mm ²	0.099 / 0.0796 / 0.102
R.F-System (2nd stage)		
Energy loss per turn	keV	580
R.F-power	kW	413
Cavity Shunt impedance	MΩ	3.4
R.F-cavity voltage	kV	487

4.2.2 The Lattice Optimisation

To get a high machine performance represented by a high brilliance, a high beam stability and lifetime, the optics should be well optimised by going through different optimisation steps.

First Step: The Optical Functions: In this part of optimisation, one try to get the required optics which achieve a small emittance, a relatively high β_x in the injection section (to ease the injection process), a small β_z in the insertion device section (to minimize their unwanted optical effects), a relatively low β_x and β_z in the quadrupoles (to minimize the natural chromaticities) and other aspects that guarantee the high brilliance and beam stability.

Second Step: Choosing the Working Point: The first step should be accompanied by a good choice for the machine tunes. The working point should be chosen in a region, on the tune diagram, where the minimum destructive resonances which threat the beam stability and lifetime. The tunes have to achieve the minimum sensitivity to dipolar and quadrupolar errors. It is recommended for the vertical tune to be below the half integer in order to reduce resistive wall instabilities.

Third Step: Optimising the Tune Shift with Amplitude and the Dynamic Aperture: The tune shift with amplitude is the unwanted effect of the chromatic sextupoles which means that position the sextupoles in suitable places in the ring will minimize this non linear effect. Minimising the tune shift with amplitude also depends strongly on the 2nd step as well as on the first step where the natural chromaticity should be minimized as much as possible. After taking the above helpful actions, the tune shift with amplitude can be minimised by optimising the sextupole strengths.

This optimisation will result in increasing the transverse stable area provided for the beam oscillation, i.e. increasing the dynamic aperture which should be larger than the physical one.

Fourth Step: Studying the Machine Acceptance: Since the dynamic aperture calculations determine the boundary of the dynamic aperture, testing the stability inside it is an important procedure. This can be done by tracking a particle at several points in the horizontal and vertical phase-space for enough number of turns. The shapes of the resulted ellipses will denote the strength of non linearity, and the presence of any respected resonance will be revealed.

Fifth Step: Studying the Off-momentum Dynamics: As the stability of the off-momentum particles will provide a relaxed Touschek and Bremsstrahlung lifetimes, a great interest should be given to this part.

The tune shift with momentum deviation is a result of the non linearity caused by the sextupoles. This tune shift can't be well controlled, but it depends strongly on the working point and the value of the natural chromaticity (the 1st and 2nd steps) as well as on the value of corrected chromaticity. It is of great deal that the tune of the off-momentum particles doesn't cross any destructive resonance as well as the tune shift with amplitude of these particles. A good dynamic aperture for the off-momentum particle will be a result of that.

4.2.2.1 Choice of the Working Point

To avoid the instabilities, and to enhance the off-axis and off-momentum particle dynamic behaviours, the working point has been chosen to satisfy several criteria:

- a) to be where the amplitudes of the 3rd order resonance driving terms are as small as possible.
- b) to be where the tune shifts with amplitude are as small as possible.
- c) to be with fractional parts that prevent any tune coupling (equality in the tune fractional parts) before the end of the physical aperture.
- d) to be with fractional parts that offer larger momentum aperture in case of correcting the horizontal and vertical chromaticity to +2, at least.

After testing some working points with horizontal integer part of 7 and vertical ones of 4 and 5 [i.e. (7--, 4--) and (7--, 5--)], the working point with 7 and 5 as horizontal and vertical integer parts satisfied conditions a) and b) much more than that of 4 as a vertical integer part.

In order to satisfy the condition c) and due to the directions of the horizontal and vertical tune changes with amplitude (see figure (4.5)), the vertical fractional part of the tune has been chosen to be less than the horizontal one. This will help in avoiding any tune coupling may cause a betatron coupling which may lead, in turn, to unwanted effects.

Since the natural chromaticity will be corrected to 2, the tune shifts with energy will be with high slopes that cause the off-momentum particles to cross some dangerous resonance at small energy deviations causing them to be lost (see section 4.2.2.4). To avoid this risk (i.e. to satisfy condition d)), the fractional parts of the tunes have been chosen to be less than 0.23.

The chosen working point (7.217, 5.192) and its position from different types of resonance is shown on the tune diagram in figure (4.3).

The resonance lines on the tune diagram are given by the resonance equation:

$$m * Q_x + n * Q_z = k \quad (4.5)$$

Where m , n and k are integers, Q_x and Q_z are the horizontal and vertical tunes. $|m| + |n|$ is the order of the resonance.

If the integer k is a multiple of the machine periodicity (i.e. $k = L * P$, L is integer and P is the machine periodicity which is 8 in SESAME case) then the resonance is called “systematic” or “structure” resonance and could be more serious than the others of the same order. Also, the sum resonance (represented by descending lines on the tune diagram) are of greater concern than difference resonance (represented by ascending lines). The resonances of small order are more dangerous than that of high order, so the integer, half-integer and third-integer resonance are the most serious ones which should be avoided.

The resonance lines and their driving forces, up to 7th order, are given by table (4.3), and the preliminary analysis to the closest resonance lines surrounding the working point are given in table (4.4) and their indications are shown in figure (4.4).

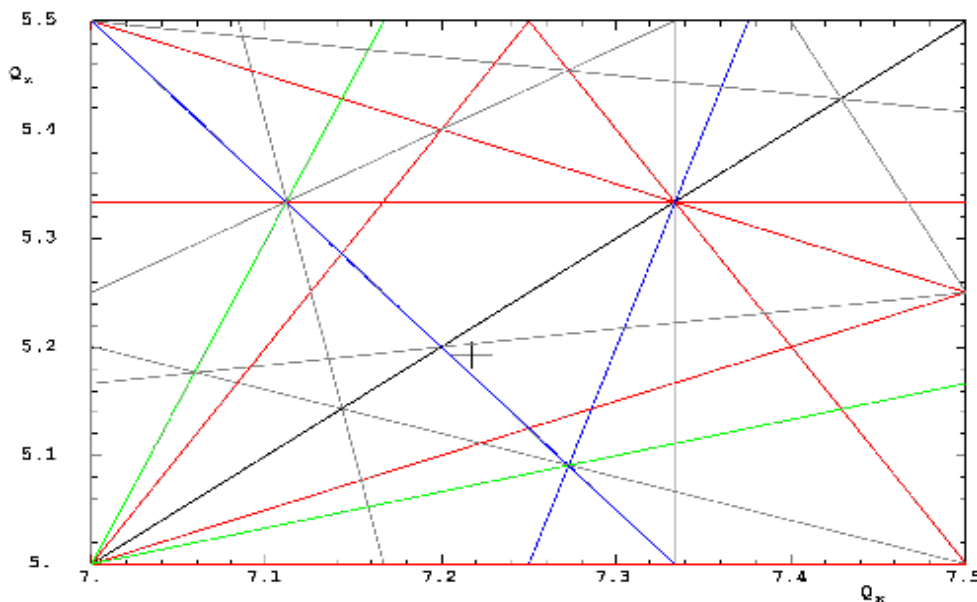


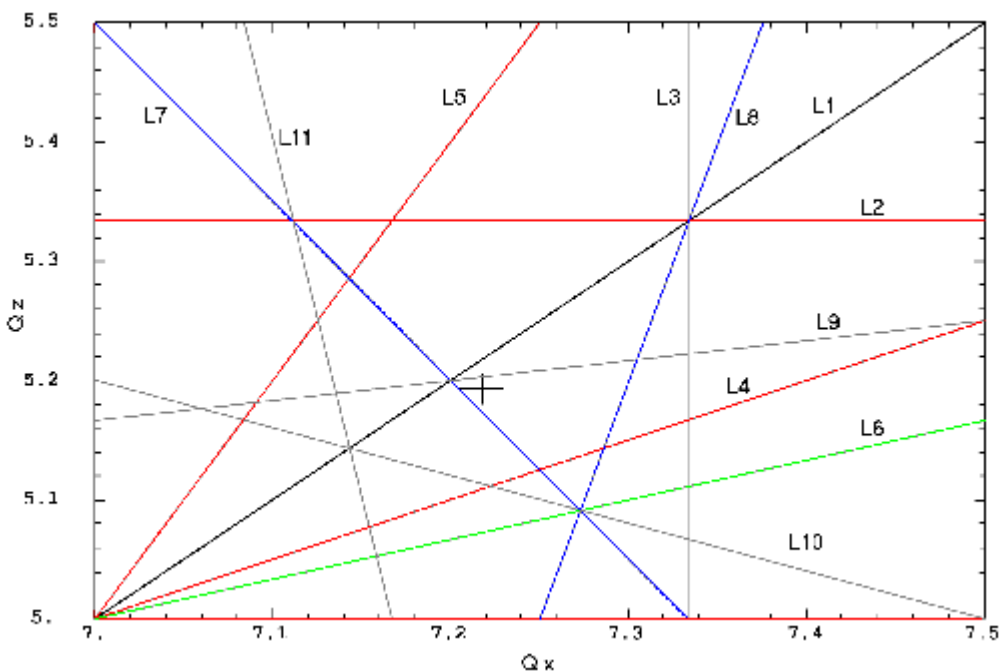
Figure 4.3: Tune diagram shows all the 2nd order (in black) and 3rd order (in red) resonance as well as the systematic 4th (in green), 5th (in blue) and 7th (in grey) order resonance.

Table 4.3: Resonance lines and their driving forces up to 7th order.

Resonance order	Driving multipole	Resonance lines caused by normal multipole	Resonance lines caused by skewed multipole	Number of lines
Integer	Dipole	$Q_x = k$	$Q_z = k$	2
Half-integer	Quadrupole	$2Q_x = k$, $2Q_z = k$	$Q_x \pm Q_z = k$	4
Third-integer	Sextupole	$3Q_x = k$, $Q_x \pm 2Q_z = k$	$2Q_x \pm Q_z = k$, $3Q_z = k$	6
Fourth-integer	Octupole	$4Q_x = k$, $2Q_x \pm 2Q_z = k$ $4Q_z = k$	$3Q_x \pm Q_z = k$ $Q_x \pm 3Q_z = k$	8
Fifth-integer	Decapole	$5Q_x = k$, $3Q_x \pm 2Q_z = k$ $Q_x \pm 4Q_z = k$	$2Q_x \pm 3Q_z = k$ $4Q_x \pm Q_z = k$, $5Q_z = k$	10
Sixth-integer	dedecapole	$6Q_x = k$, $4Q_x \pm 2Q_z = k$ $2Q_x \pm 4Q_z = k$, $6Q_z = k$	$5Q_x \pm Q_z = k$ $3Q_x \pm 3Q_z = k$ $Q_x \pm 5Q_z = k$	12
Seventh-integer	14-pole	$7Q_x = k$, $5Q_x \pm 2Q_z = k$ $3Q_x \pm 4Q_z = k$ $Q_x \pm 6Q_z = k$	$6Q_x \pm Q_z = k$ $4Q_x \pm 3Q_z = k$ $2Q_x \pm 5Q_z = k$, $7Q_z = k$	14

Table 4.4: Resonance lines around the working point (see figure (4.4)).

Name	Resonance line	Order	Driving source	Gravity
L1	$Q_x - Q_z = 2$	2 nd	Skew quadrupole	Near by, not dangerous
L2	$3Q_z = 2*8$	3 rd	Skew sextupole	Far away, not dangerous
L3	$3Q_x = 3*8$	3 rd	Normal sextupole	Far away, not dangerous
L4	$Q_x - 2Q_z = -8$	3rd	Normal sextupole	Medium distance, could be dangerous
L5	$2Q_x - Q_z = 9$	3rd	Skew sextupole	Far away, not dangerous
L6	$Q_x - 3Q_z = -8$	4th	Skew octupole	Far away, not dangerous
L7	$3Q_x + 2Q_z = 32$	5th	Normal decapole	Near by, not dangerous
L8	$4Q_x - Q_z = 3*8$	5th	Skew decapole	Medium distance, not dangerous
L9	$Q_x - 6Q_z = -3*8$	7th	Normal 14-pole	Near by, not dangerous
L10	$2Q_x + 5Q_z = 5*8$	7th	Skew 14-pole	Medium distance, not dangerous
L11	$6Q_x + Q_z = 6*8$	7th	Skew 14-pole	Medium distance, not dangerous

**Figure 4.4: The working point among the resonance lines indicated by table (4.4).**

According to table (4.4) and figure (4.4), the only resonance line that could have a serious danger is L4, but the working point is not expected to reach this line (see section 4.2.2.2) which makes it out of the dynamic range.

4.2.2.2 The Tune Shift with Amplitude

The tune shifts with amplitude were kept as smooth as possible with a special care given to the horizontal one due to the fact that the large betatron excursions will be in the horizontal plane. The choice of the working point together with the non linear optimisation were done in order to prevent the tunes from crossing any 2nd, 3rd, 4th or 5th order resonance before an enough betatron amplitude in each plane independently. They are shown in figure (4.5) for a particle tracked for 1000 turns. The horizontal shifted tune with x, at z = 0, reach the random 4th order resonance ($Q_x = 7.25$) after 40 mm amplitude which is already out of the vacuum chamber ($x = 35\text{mm}$ and $x = -27.5\text{mm}$ where the septum sheet will be) and the 3rd order resonance will be automatically far out of our range.

Concerning the vertical shifted tune, at $x = 0$, it will be changed by a small amount in the needed vertical dimension ($z = 3\text{ mm}$) where the tune will not go below 5.185.

The tune shift with horizontal and vertical amplitudes simultaneously can be seen by Frequency Map Analysis, which needs a special later study.

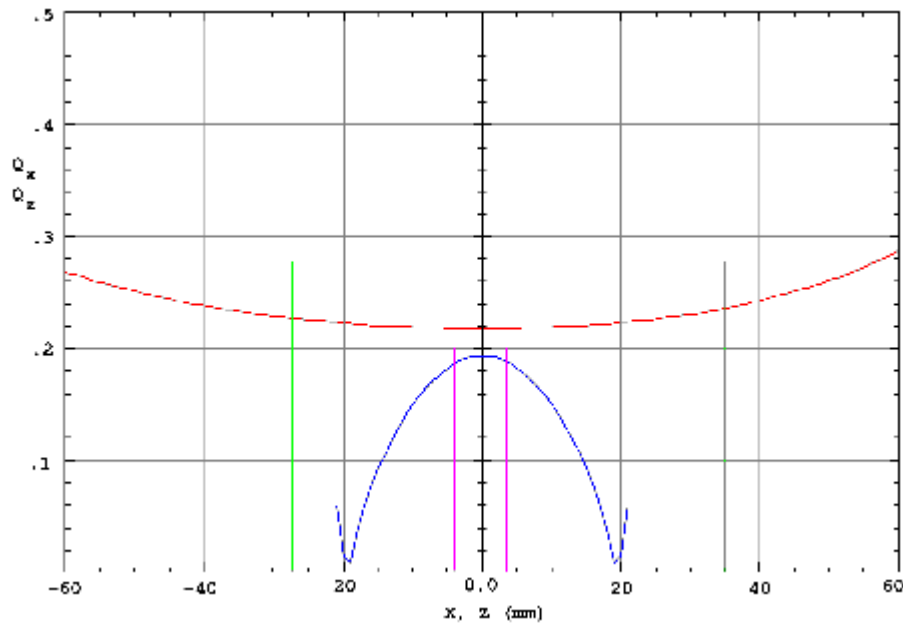


Figure 4.5: Tune shift with betatron amplitude with chromaticity = 2 in both planes. The horizontal (in red) tune is with integer part = 7 and the vertical one (in blue) is with integer part = 5. The green lines represent the horizontal limiting aperture, while the pink lines represent the vertical limiting aperture.

4.2.2.3 The Dynamic Aperture

The dynamic aperture is the stable transverse area for the particle in which it can execute its oscillations safely without getting defused or lost, the boundary of the dynamic aperture separates between the stable and unstable regions. It should be larger than the vacuum chamber to guarantee a good beam lifetime.

A large dynamic aperture is an indication of high beam stability and it is the result of the linear and non linear optimisations where the oscillating particle is protected from falling into any significant resonance before an enough amplitude. Figure (4.6) shows the dynamic aperture compared to the needed physical one.

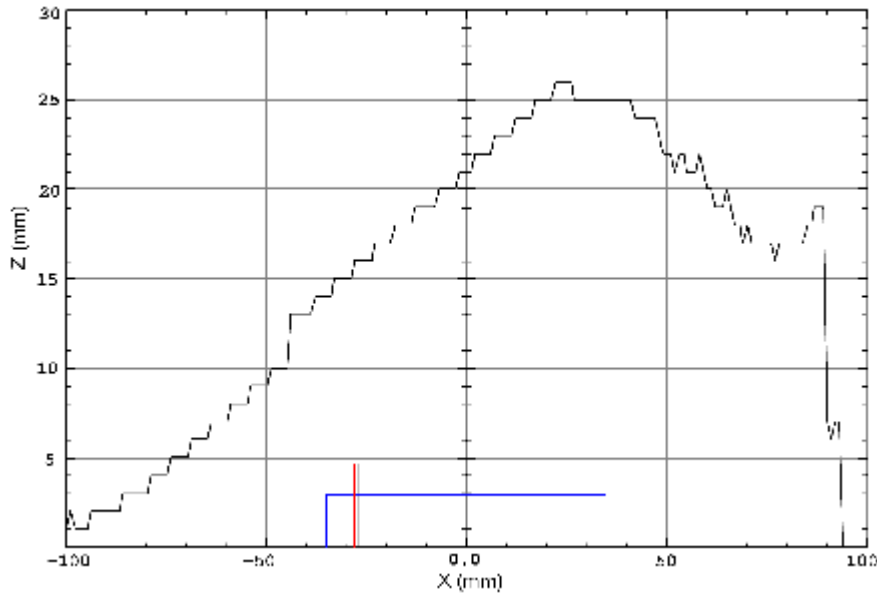


Figure 4.6: Dynamic aperture (in black) for on-momentum particle, calculated for 1000 turns. Physical aperture is shown in blue while the septum sheet (at $x = -27.5\text{mm}$) is represented by the red line.

For more trustable results, the on-momentum particle has been tracked for 1000 turns at each 5 mm in the horizontal phase space ($z = 0$) and at each 2 mm in the vertical phase space ($x = 0$). Figure (4.7) shows the normalized horizontal phase space tracking that attests the stability of the particles up to $x = 75$ mm although they start a small diffusion at $x = 55$ mm, which is already out of the vacuum chamber ($x = 35\text{mm}$ and $x = -27.5\text{mm}$ at septum). It should be noted here that the normalized phase space is a transformation of the normal one where the phase space ellipse becomes a circle. The Courant-Snyder invariant is treated as:

$$\gamma y^2 + 2\alpha y y' + \beta y'^2 = \varepsilon \quad \Rightarrow \quad y^2 + (\alpha y + \beta y')^2 = \beta\varepsilon, \quad \text{where } y \text{ represents } x \text{ or } z.$$

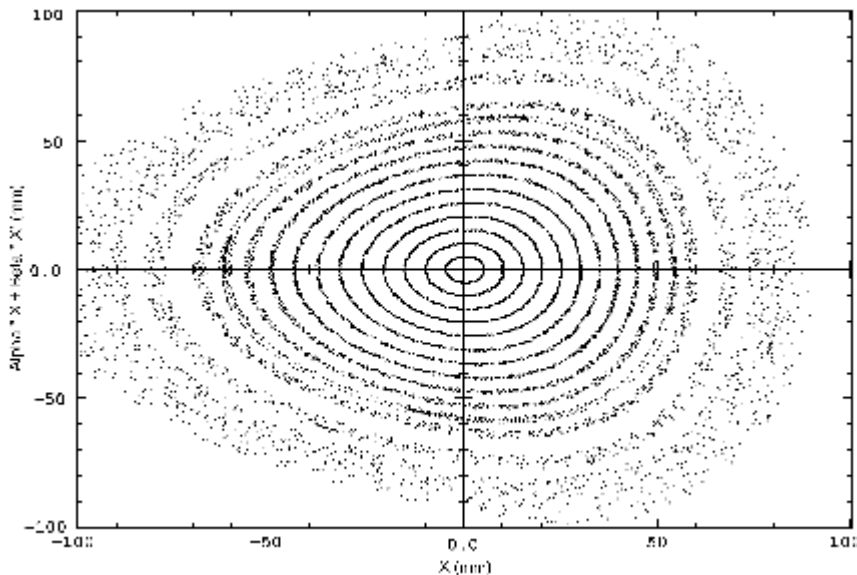


Figure 4.7: The normalized horizontal phase space at $z = 0$.

The low deformation of the ellipses which start after $x = 25$ mm shows the beginning of the weak resonance effects effect at that amplitude.

The normalized vertical phase space at $x = 0$ is shown in figure (4.8) where the regular shapes of the ellipses up to $z = 16$ mm attests the stability in this region. The unstable region starts after $x = 18$ mm where the particles start to diffuse.

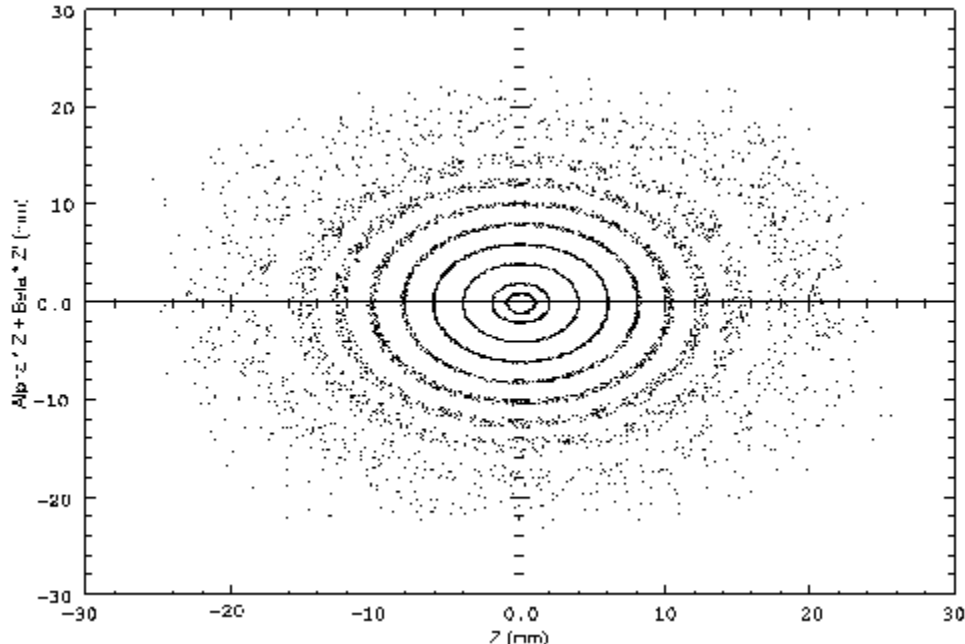


Figure 4.8: The normalized vertical phase space at $x = 0$.

These calculations have been done at the beginning of the super period where the needed vertical half-aperture is 3 mm.

4.2.2.4 The Off-momentum Dynamics

The collisions happen between the beam particles cause energy transfers (loss or gain) between them and they start to execute oscillations in energy. Due to the chromaticity value and the sextupole non linear effects, the tunes become energy dependant.

Protecting these off-momentum particles from being lost has a great concern in keeping a reasonable beam lifetime.

An attention was paid to keep the shifted tune with energy away from crossing the dangerous resonance especially the 3rd order one. Because the optimisation was for a corrected chromaticity = 2 in both planes, the slope of the tune shift with energy deviation was high i.e. the tune changes highly with energy deviation. This causes the shifted tune to cross different significant resonances before the particle reach an enough energy deviation that guarantees reasonable Touscheck and Bremsstrahlung lifetimes. This risk was avoided by choosing the fractional parts of the tunes to be below (0.23) which guarantees that the off-momentum particles will not cross the 3rd order resonance before a 3% of momentum deviation, as shown in figure (4.9). We need this high momentum aperture so far.

In non-zero dispersion section (which is everywhere in SESAME ring), the off-momentum particles will oscillate around different off-momentum closed orbits displaced from the nominal one by a distance Δx depending on the particle momentum deviation and the dispersion value η_x :

$$\Delta x = \eta_x \cdot \Delta p / p \quad (4.6)$$

The oscillation of the off-momentum particles in energy means their oscillation between the average amplitudes $\pm \Delta x$ from the nominal orbit, which makes it necessary to check their

tune shift with amplitude. Figure (4.10) shows the tune shift with amplitude for particles with momentum deviation between 4% and -4%. Taking into account the positions of the different off-momentum closed orbits from the vacuum chamber centre, together with the borders of the vacuum chamber at $x = \pm 35$ mm, we see that none of these particles crosses any destructive resonance like the 3rd order one.

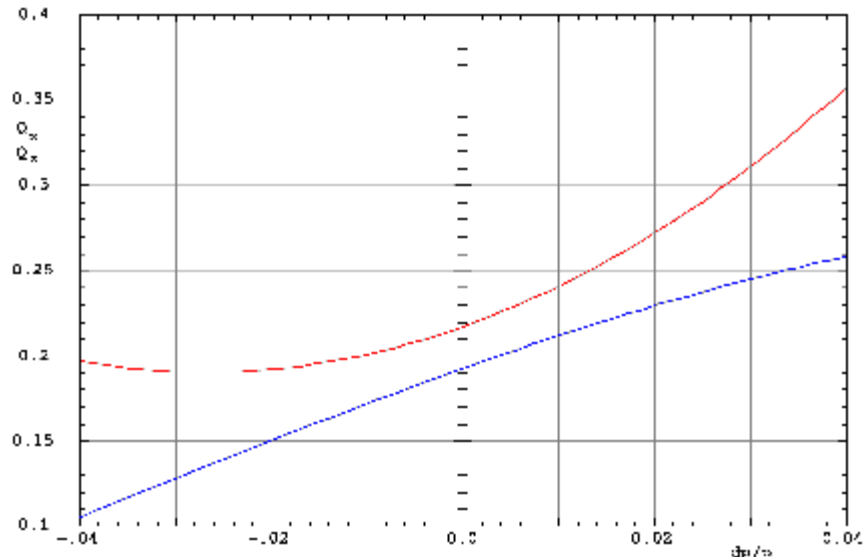


Figure 4.9: Horizontal (in red) and vertical (in blue) tune shifts with momentum deviation. Corrected chromaticity = 2 in both planes.

Dynamic apertures, around the axis of the vacuum chamber, for the particles with momentum deviation between 4 % and -4% are shown in figure (4.11). Oscillation of these particles around different closed orbits must be also taken into account in figure (4.11).

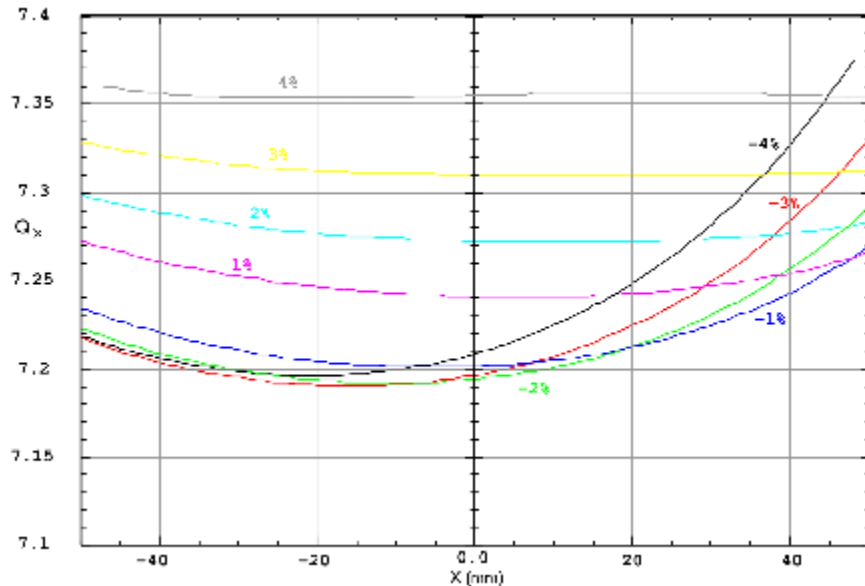


Figure 4.10: The tune shift with amplitude for the off-momentum particles with momentum deviation of : 4%(grey), 3%(yellow), 2%(cyan), 1%(pink), -1%(blue), -2%(green), -3%(red) and -4%(black).

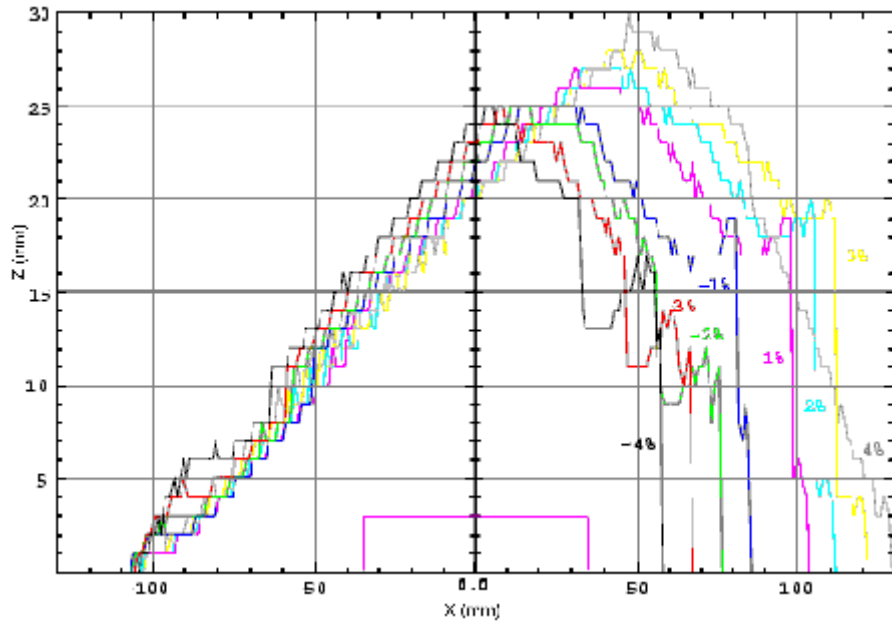


Figure 4.11: Dynamic apertures for off-momentum particles of 4% (grey), 3% (yellow), 2% (cyan), 1% (pink), -1% (blue), -2% (green), -3% (red) and -4% (black). The needed physical acceptance appears in pink.

Tracking the extreme off-momentum particles of $\Delta p/p = 4\%$ and -4% , as an example, around their closed orbits in the horizontal and vertical phase spaces, shows the stability of these particles inside the vacuum chamber. This is shown by figures (4.12), (4.13), (4.14) and (4.15).

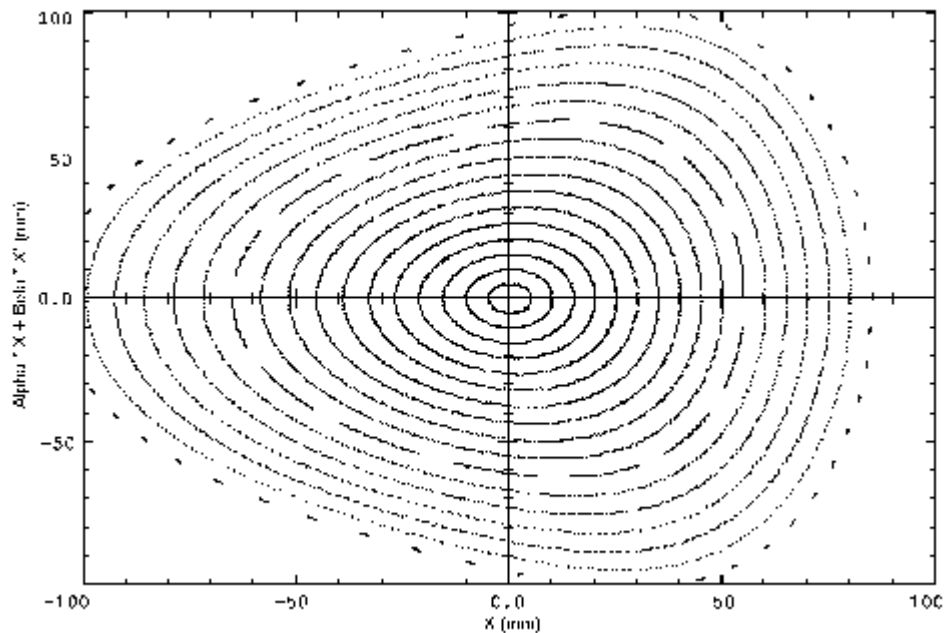


Figure 4.12: Tracking of the 4% off-momentum particle, around its chromatic orbit, in the normalized horizontal phase space.

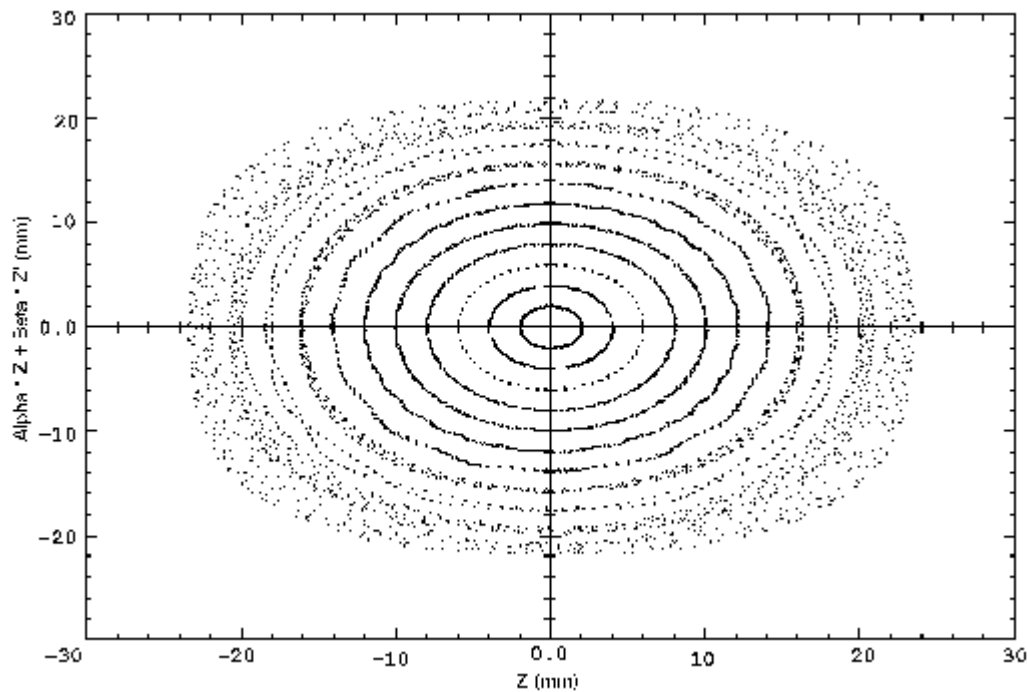


Figure 4.13: Tracking of the 4% off-momentum particle in the normalized vertical phase space.

The high order resonance at $x = 55\text{mm}$ in figure (4.12), $x = 25\text{mm}$ in figure (4.14) and the 4th order one at $z = 4\text{mm}$ in figure (4.13) are not dangerous since they are followed by stable regions.

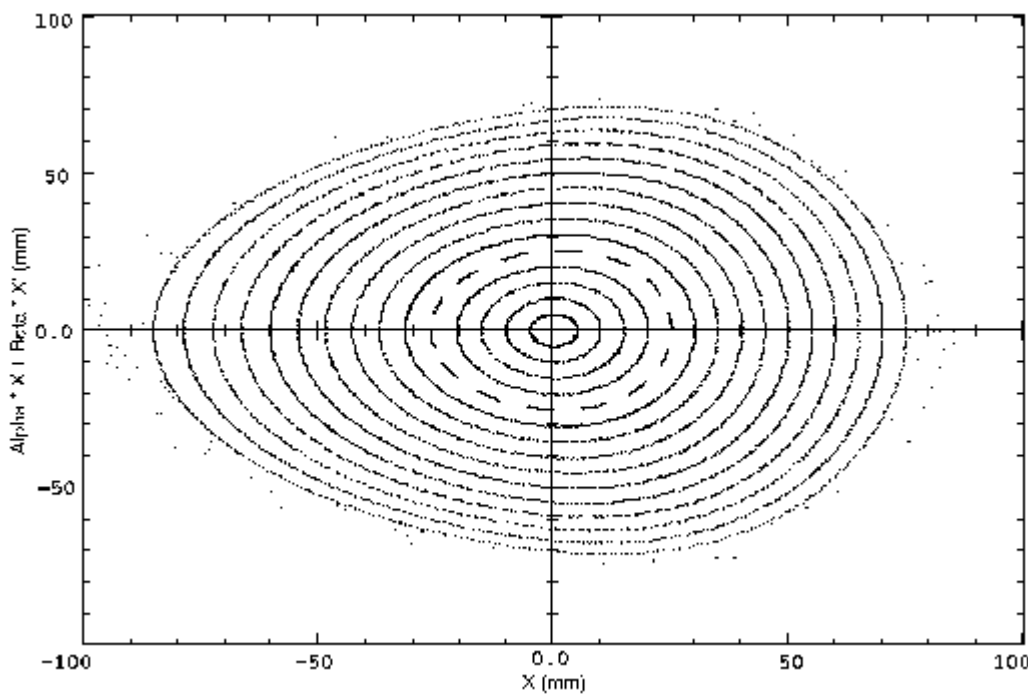


Figure 4.14: Tracking of the - 4% off-momentum particle, around its chromatic orbit, in the normalized horizontal phase space.

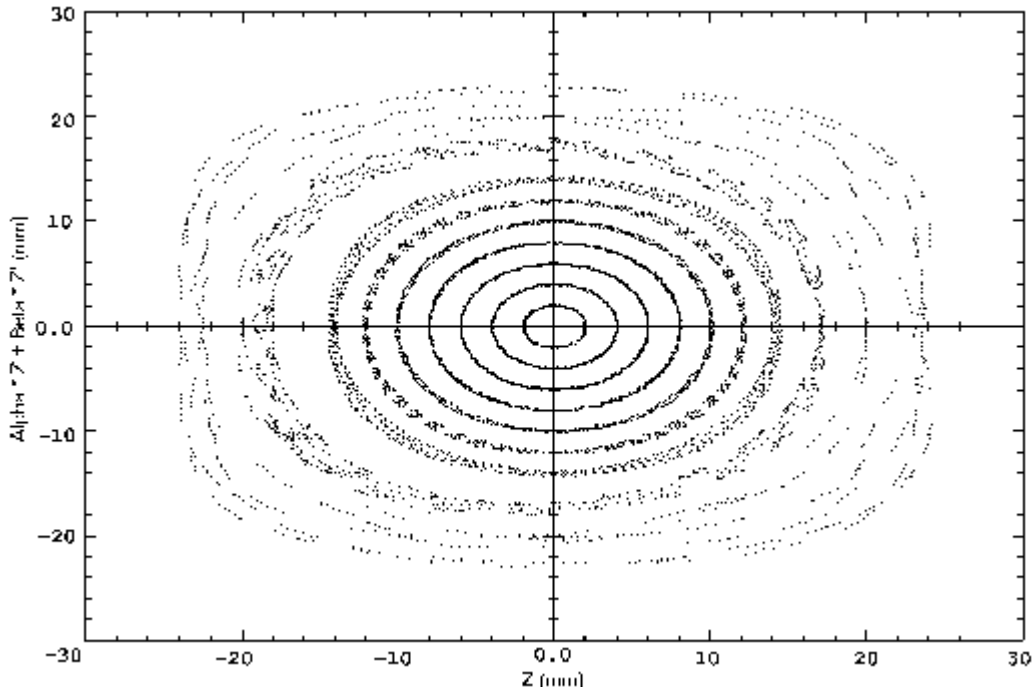


Figure 4.15: Tracking of the - 4% off-momentum particle in the normalized vertical phase space.

4.2.3 The Machine Acceptance

The physical acceptance at some point (s) in the ring is defined by the maximum emittance that can be accepted at that point. It depends on the optical functions, the particle momentum deviation and on the transverse limiting aperture there. It can be determined by the vacuum chamber or the dynamic aperture dimensions. The physical acceptance of the machine is determined by the minimum acceptance all over the ring i.e. the minimum of the maximum emittance accepted by the ring:

$$A_{\text{phys}}(\delta)_{x,z} = \text{Min}\{(Y_{x,z}(s) - \eta_{x,z}(s) * \delta)^2 / \beta_{x,z}(s)\} \quad (4.7)$$

Where $Y_{x,z}(s)$ is the limiting dimension which could be the vacuum chamber aperture or the dynamic aperture and $\delta = \Delta p/p$ is the particle momentum deviation.

In SESAME case and without introducing the multi-polar effects (the ideal machine case), the machine physical acceptance is limited by the vacuum chamber acceptance as shown by figure (4.16). The calculations have been done at the beginning of the ring where the septum will be. One can hope that the dynamic acceptance will still larger than the chamber one under the multi-polar effect in case if the magnetic elements were well manufactured.

The machine physical acceptance is always limited horizontally by the septum magnet position if it is at $x < 34.6$ mm from the axis of the vacuum chamber. On the condition that the septum will be at $x = -27.5$ mm, the horizontal acceptance (for the on-momentum particle) = $6.94 \cdot 10^{-5}$ mrad. Vertically, it will be limited by the in-vacuum undulator gap (3 mm), which makes the vertical acceptance to be $5.2 \cdot 10^{-6}$.

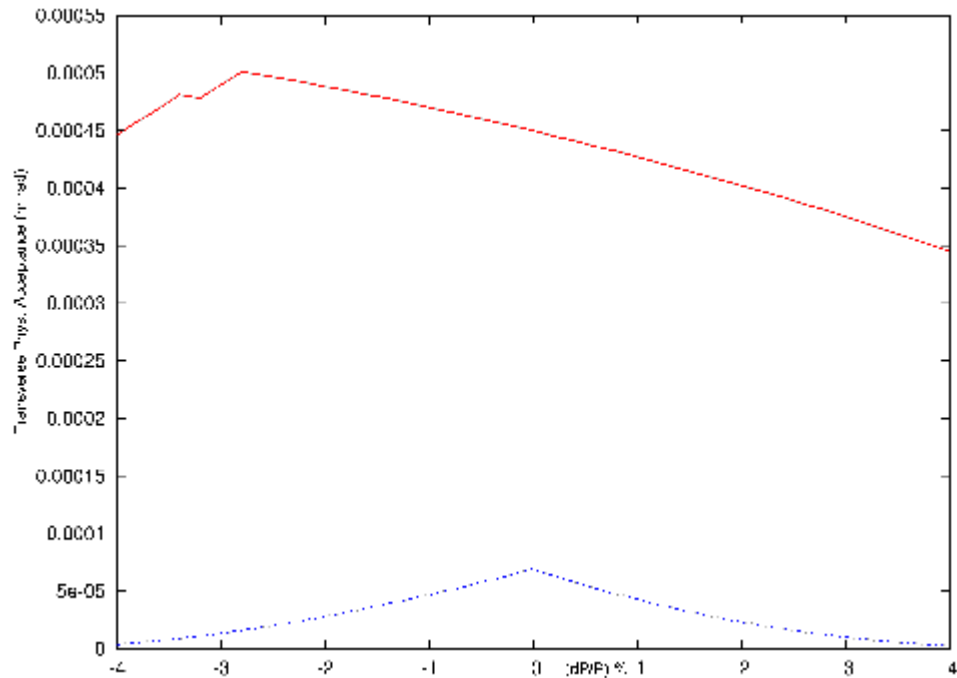


Figure 4.16: The ideal dynamic acceptance (in red) and the physical one determined by the vacuum chamber (in blue) as a function of δ .

The energy acceptance (momentum aperture) at some point (s) is the maximum energy deviation given to the particle at that point without causing it to get lost anywhere in the ring. At some point (s), the energy acceptance is limited longitudinally by the RF energy one and transversely by the min [chamber energy acceptance, the dynamic aperture one].

In the transverse plane, the energy acceptance at some deviation point depends on the Twiss parameters (α, β, γ) and the dispersion (η) of the deviated particle at that point as well as on the β, η and the limiting transverse dimension (the vacuum chamber or the dynamic aperture) at any other point in the ring.

The transverse energy acceptance at any collision point (s^*) (which produce the particle energy deviation δ) in the ring, can be calculated from the following equation:

$$\varepsilon_{t,acc}(s^*, \delta) = X(s) / [\eta(s) + [\beta(s) H(s^*, \delta)]^{1/2}] \quad (4.8)$$

and: $H(s^*, \delta) = \gamma(s^*, \delta) \eta^2(s^*, \delta) + 2 \alpha(s^*, \delta) \eta(s^*, \delta) \eta'(s^*, \delta) + \beta(s^*, \delta) \eta'^2(s^*, \delta)$

Where $X(s)$ is the limiting transverse aperture at some point (s) and $H(s^*, \delta)$ is the energy-dependant lattice invariant (H-function) of the collided particle at point (s^*).

Generally, the energy acceptance = min [RF energy acceptance, vacuum chamber energy acceptance, dynamic aperture energy acceptance]. Since the dynamic acceptance is much larger than the chamber one, as shown in figure (4.16), we are limited transversely always by the vacuum chamber (specifically by the septum magnet).

Figure (4.17) shows the change in the transverse energy acceptance, according to equation (4.8), along one super period of SESAME ring. The positive energy acceptance ($\Delta p/p \%$) is shown in blue while the negative one ($-\Delta p/p \%$) is shown in red. It can be seen that the minimum energy acceptance is at the middle of the bending magnet and it is about 2.17 % in the positive side of the chamber and about -2.32 % in the negative side of the chamber.

The difference in energy acceptance between the positive deviation and the negative one is a result of the non linearity caused by the sextupoles (see figures (4.7), (4.12) and (4.14)) which cause the corresponding total amplitude of the positively deviated particle to be different from

that of the negatively deviated one, specifically at the points of high amplitudes. This will make the deviated particles see different limitations at the same point which determines, in turn, different energy acceptances (for $+\delta$ and $-\delta$) at the same collision (deviation) point. In the ideal case the energy acceptance should be symmetric around the nominal closed orbit (the vacuum chamber axes).

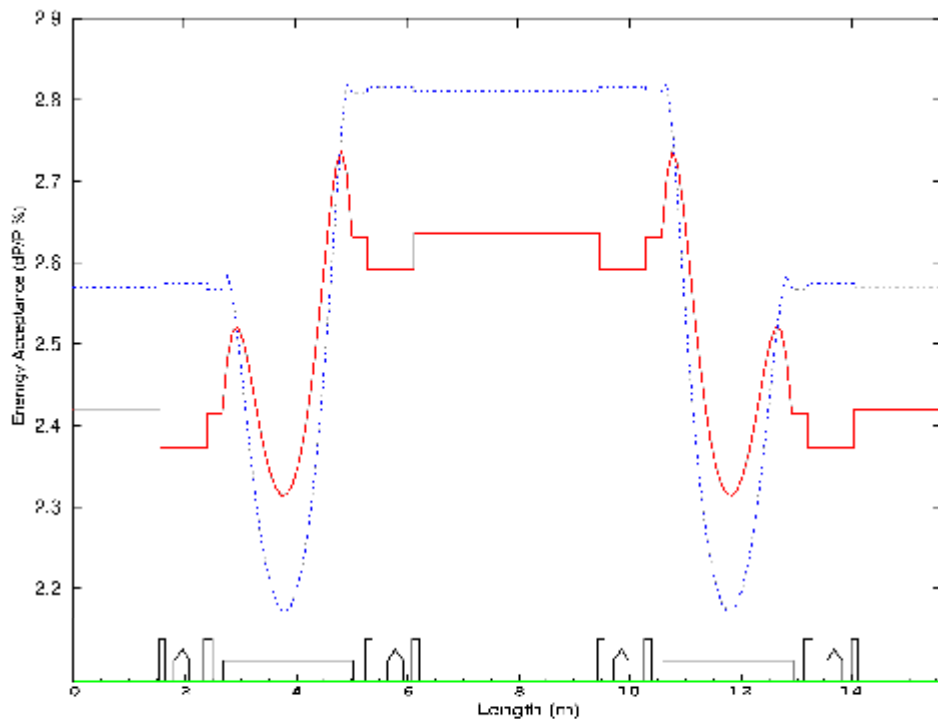


Figure 4.17: The absolute energy acceptance change through the super period of SESAME ring. The positive energy acceptance is in blue and the negative one is in red.

Getting the minimum energy acceptance to be in the bending is a result of the fact that the maximum H-function is in the middle of the bending and this is due to the high dispersion value there (0.137m). This high dispersion value in the bending centre –in spite of the dispersion distribution in the straight sections- is a consequence of the large bending angle (0.393rad). Figure (4.18) shows the energy-dependant H-function ($H(s, \delta)$) along one super period of SESAME storage ring.

Since the RF energy acceptance of SESAME will be around 1.3 % at the beginning, the machine energy acceptance will be limited only by the RF one.

A high energy acceptance is necessary to accommodate a good percentage of the off-momentum particles which will lead to a comfortable Touschek and Bremsstrahlung lifetimes.

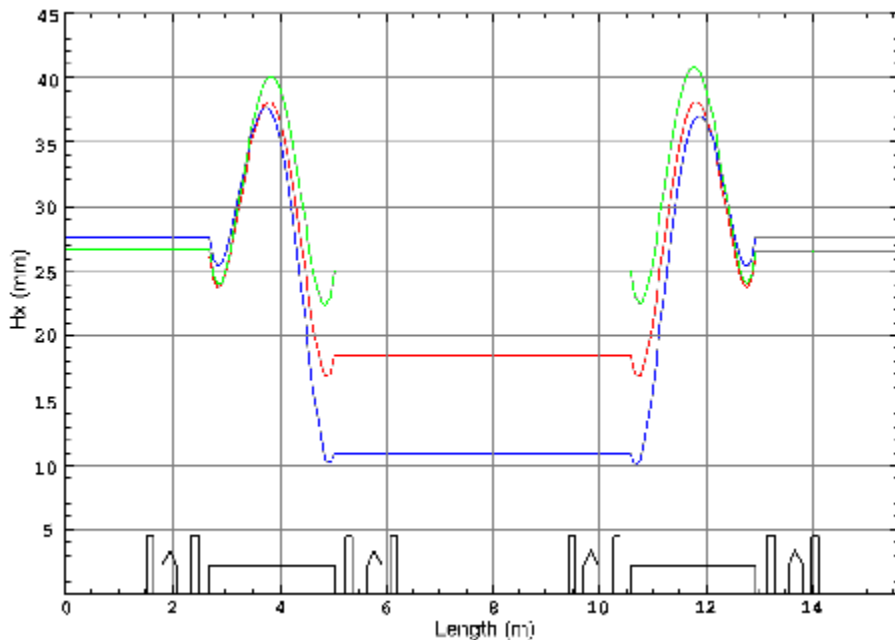


Figure 4.18: The horizontal $H(s, \delta)$ function (see equation 4.8) along one super period for: the on-momentum particle (in red), the 2% (in blue) and the -2% (in green) off-momentum particles.

4.3 Effect of Insertion Devices on SESAME Optics

4.3.1 Choosing the Optimum Optics

Getting high energy photons together with a high brilliance is of high priority in SESAME as well as the synchrotron light sources. Since this radiation with these characteristics can be provided by the insertion devices (IDs), SESAME machine is considered as a machine of insertion devices. This made studying their effect on the beam optics, and testing the flexibility of the ring lattice in dealing with them a crucial issue in SESAME life.

As wigglers have stronger effects on beam dynamics than undulators, our preliminary study on the IDs effects and their treatments has been concentrated on them.

The beam optics behaviour under wiggler effect has been investigated using two types of wigglers:

- **One with:** magnetic field = 2.5T, length = 2.4m and period length = 120mm.
- **The other with:** magnetic field = 3.5T, length = 1.44m and period length = 60mm.

The dispersion in the wiggler straight section has a principal role in determining the wiggler effect on the emittance which has its direct effect on the beam size (σ_x) and divergence (σ'_x). Since the brilliance of the wiggler radiation is inversely proportional to the beam size and beam divergence in the wiggler, the value of dispersion there has a strong effect on the brilliance value.

For the sake of finding the optimum optics for different IDs configurations, different optics of different dispersion values (in the wiggler section) have been investigated using cases of 2, 4 and 8 wigglers inserted. These cases are preferable due to their compatibility with SESAME ring symmetry as has been shown in the previous “White Book”. The corresponding quadrupole and sextupole strengths to the investigated optics are given by table (4.5) while table (4.6) shows the different optics emittances before and after applying wigglers in the above cases.

A comparison was made between the different optics for the highest wiggler radiation brilliance for the above wiggler types and number cases. Figures (4.19) and (4.20) show the brilliance comparison for the two types of wigglers in 8 wigglers case.

In case of 4 and 2 wigglers, the brilliance was calculated after the compensation for beta beating and tune shift has been done. That was due to the small optical changes happen after compensation.

On the other hand, the dispersion change in wiggler section changes the dispersion in the undulator section which changes, in turn, the beam size and divergence there. This will affect the brilliance of the undulator radiation which is inversely proportional to the quantity $\sigma_x * \sigma'_x$ (in the electron beam limit). The increase in the wiggler-section dispersion decreased both of the beam size and divergence. This has been taken into account in choosing the optimum optics.

Table 4.5: The quadrupole and sextupole strengths of the investigated optics with different dispersion values in the wiggler straight section.

Optics of dispersion (cm)	k-value of quad Q1 (m ⁻²)	k-value of quad Q2 (m ⁻²)	m-value of sextupole S1 (m ⁻³)	m-value of sextupole S2 (m ⁻³)	m-value of sextupole S3 (m ⁻³)	m-value of sextupole S4 (m ⁻³)
0	2.08714	1.985	9.9	- 13.9	- 11.37	8.34
10	2.0764	1.99403	9.873	- 13.713	-11.372	8.365
16	2.0696	1.9999	9.76	-13.57	-11.723	8.38
19	2.06663	2.0026	9.71	- 13.518	- 11.781	8.41
22	2.06338	2.00552	9.66	- 13.469	- 11.8276	8.435
26	2.05895	2.00952	9.55	- 13.4	- 11.943	8.6117
30	2.0546	2.0135	9.4286	- 13.283	- 12.1272	8.7655
35	2.04916	2.0186	9.4491	- 13.214	- 12.1896	8.6292

Table 4.6: The emittance of different optics with and without wigglers. ϵ_0 is the emittance without wigglers, ϵ_w is the emittance after applying wigglers and $\epsilon_{eff} = \sigma_x * \sigma'_x$.

Dispersion value in the wiggler section (cm)	ϵ_0 (nm.rad)	8 wigglers				4 wigglers				2 wigglers			
		B= 2.5T		B= 3.5T		B=2.5T		B=3.5T		B=2.5T		B=3.5T	
		ϵ_w (nm.rad)	ϵ_{eff} (nm.rad)	ϵ_w	ϵ_{eff}								
0	45.7	31	31	29	29	35.8	35.8	34.7	34.7	39.4	39.4	38.7	38.7
10	38	26.4	26.9	25.5	26	30.5	31	30	30.6	34	34.5	33.6	34.1
16	34.5	25.1	26.4	24.8	26.3	28.3	29.6	28.2	29.7	31.1	32.4	30.9	32.3
19	32.8	24.7	26.5	24.8	27	27.6	29.4	27.8	29.9	30	31.8	30	32
22	31.3	24.5	26.9	25.1	28	27	29.4	27.5	30.3	29	31.4	29.2	31.8
26	29.5	24.6	27.9	26	30	26.5	29.8	27.6	31.5	27.9	31.2	28.3	32
30	28	25.1	29.5	27.3	32.6	26.4	30.8	28.1	33.2	27.1	31.5	27.9	32.7
35	26.6	26.3	32.2	29.7	36.9	26.7	32.6	29.3	36.2	26.5	32.4	27.8	34.3

The dispersion change affects some machine parameters and the energy acceptance everywhere in the ring with special attention to the septum magnet position, which will take place at one of the undulator sections. But since Touscheck lifetime is directly proportional to $\sigma_x * \sigma_z * \sigma_l * \sigma'_x * \epsilon_{acc}^2$ (where σ_l is the bunch length and ϵ_{acc} is the energy acceptance), a compromise has to be done. So the Touscheck lifetime has been calculated for each optics of different dispersion value using the same septum position and RF energy acceptance.

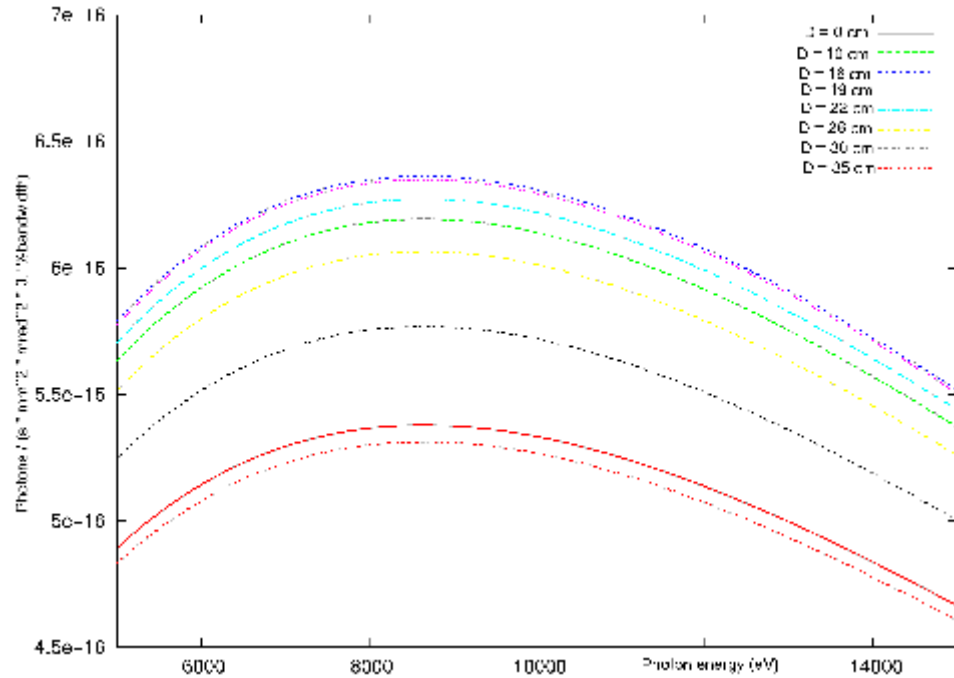


Figure 4.19: The wiggler brilliance ($B = 2.5\text{T}$, $L = 2.4\text{m}$, Period=120mm) given by optics with different dispersion (D) values from 0 to 35cm in case of 8 wigglers

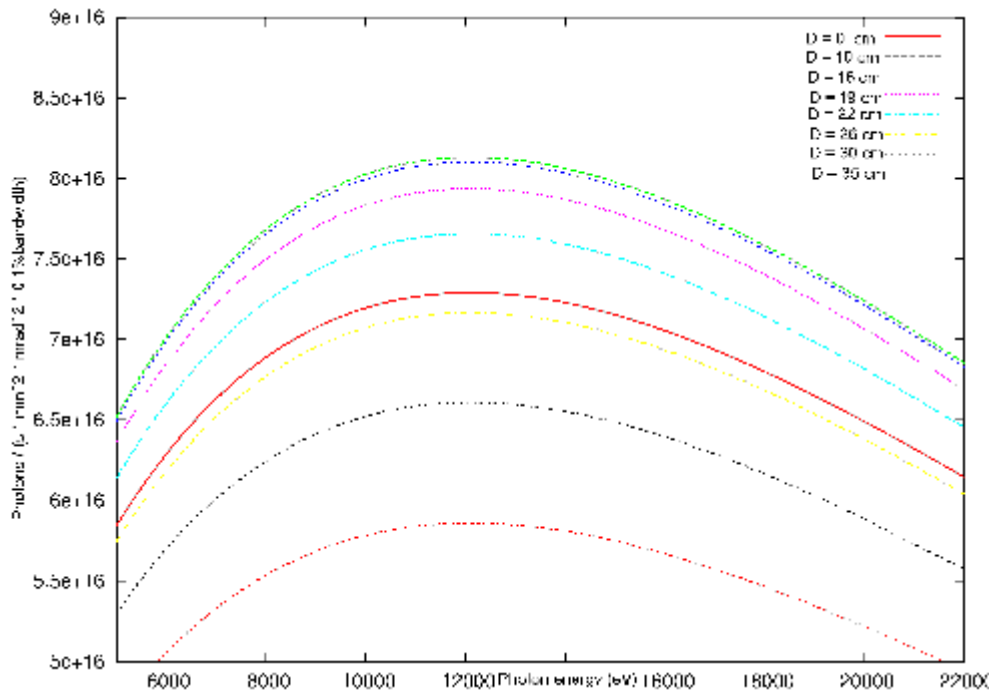


Figure 4.20: The wiggler brilliance ($B = 3.5\text{T}$, $L = 1.44\text{ m}$, Period= 60mm) given by optics with different dispersion values of 0 to 30 and 35cm in case of 8 wigglers.

The total compromise was made to choose the optics, which satisfies the conditions:

- High brilliance from the wiggler.
- High brilliance from the undulator.
- High Touschek lifetime.

for each wiggler type and each case of wiggler number.

Figures (4.21), (4.22) and (4.23) show the optimum optics of SESAME ring lattice to accommodate 2, 4 and 8 wigglers of $B= 2.5\text{T}$, $L= 2.4\text{m}$, Period= 120 mm and of $B=3.5\text{T}$, $L=1.44\text{m}$, Period= 120mm. The wiggler in all these figures will be at the middle sections.

The optics in figures (4.22) and (4.23) have been chosen on the condition that the RF energy acceptance $\leq 1.8\%$ and 1.75% respectively, otherwise the chamber energy acceptance would be less than that of the RF system which calls for another compromise to be done.

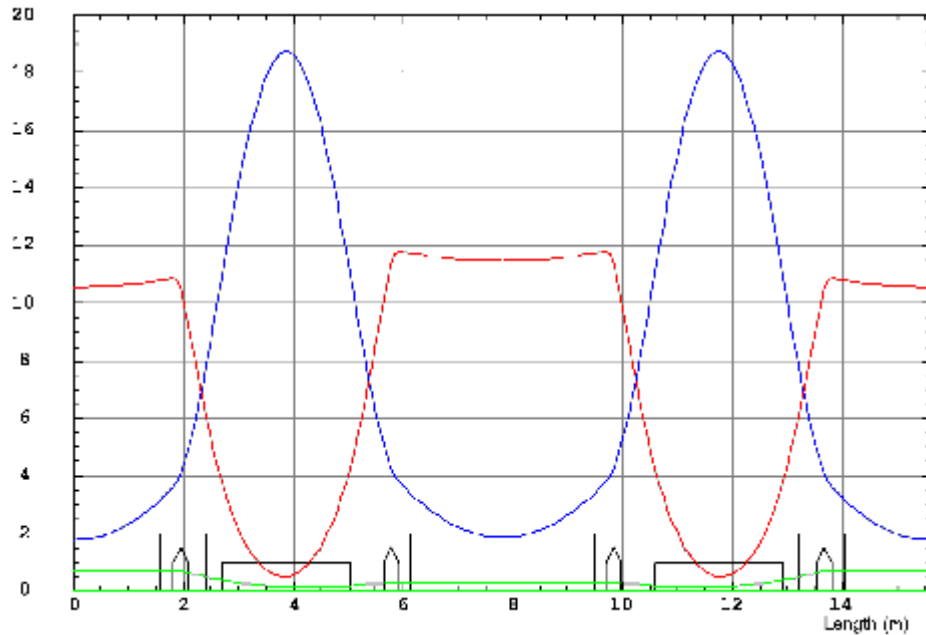


Figure 4.21: The optimum optics for 2 wigglers of both types. The dispersion in the wiggler section (in the middle) = 30cm.

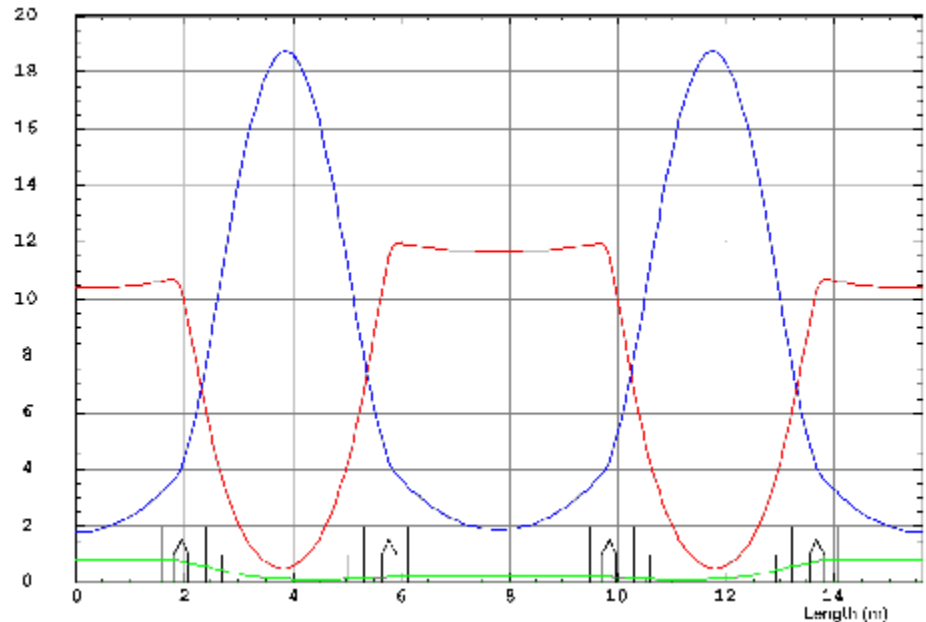


Figure 4.22: The optimum optics for 4 wigglers of both types, and 8 wigglers of $B= 2.5\text{T}$, $L= 2.4\text{m}$. The dispersion in the wiggler section = 22cm.

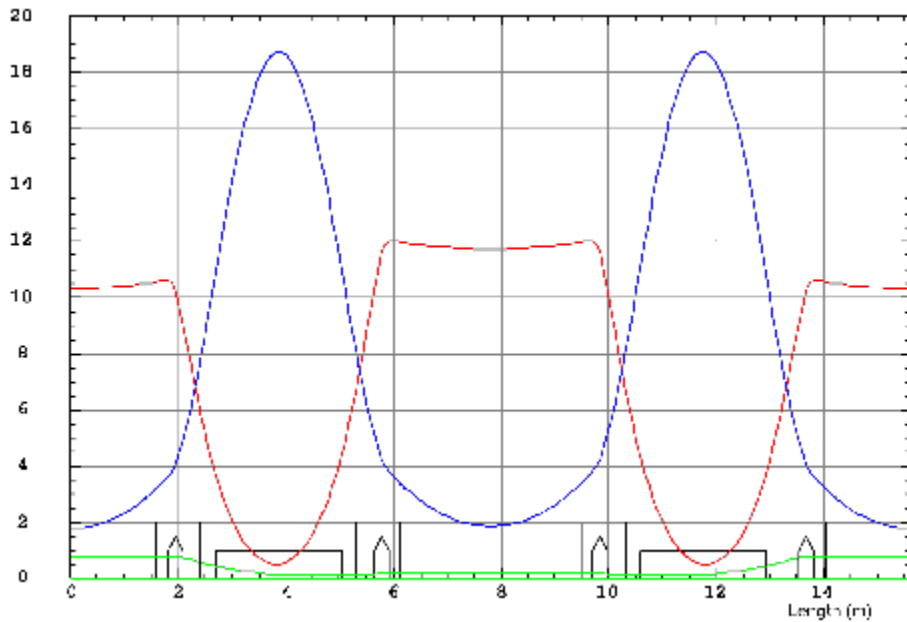


Figure 4.23: The optimum optics for 8 wiggles of $B=3.5T$, $L=1.44m$. The dispersion in the wiggler section = 19cm.

4.3.2 The Compensation for the Undesirable Effects

The undesirable effects of the IDs like vertical tune shift and beta beating, which depend on the length and the magnetic field of the ID as well as on β_z in the ID section, were reduced by the low value of β_z ($\approx 1.8m$) in the IDs straight sections. This, together with the high β_z in the BMs, had the advantage of reducing the gradient change needed to compensate for the tune shift and beta beating.

The Case of 8 Wiggles of the Same Type: In the case of 8 wiggles there was no beta beating because of the convenience between the number of magnets and the storage ring symmetry. The resulted vertical tune shift has been compensated *globally* by changing (reducing) the gradient in the BMs by a small percentage.

The gradient change needed to compensate the tune depends on the magnetic field and the length of the wiggler. Taking the case of wiggler with $B= 3.5 T$ and $L=1.44 m$, as an example, the needed gradient change to compensate for the tune shift of 0.146 was 0.946%.

The small change in the horizontal tune, due to the vertical tune compensation, has been compensated *globally* using the 2 families of horizontal focusing quadrupoles. Figure (4.24) shows the optics with 8 wiggles after tune compensation.

The dynamic aperture was positively affected by the wiggler magnetic fields which made no need to compensate for the non linear effects. Figure (4.25) shows the resulted dynamic aperture, compared to the original one, for a particle tracked for 1000 turns in 6- dimensional space.

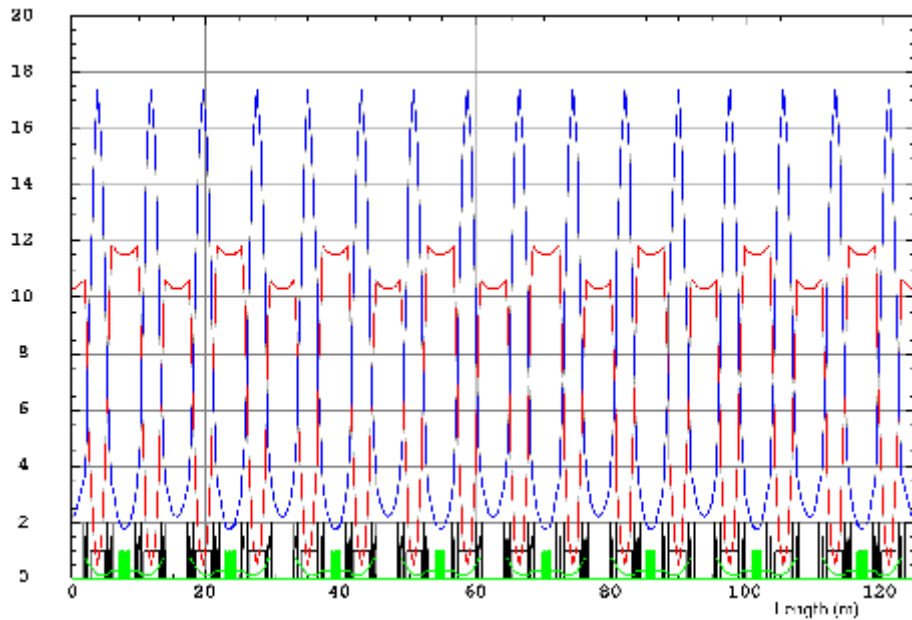


Figure 4.24: The optics with 8 wigglers of $B=3.5\text{T}$ and $L=1.44\text{m}$ after tune compensation. The total ring is shown.

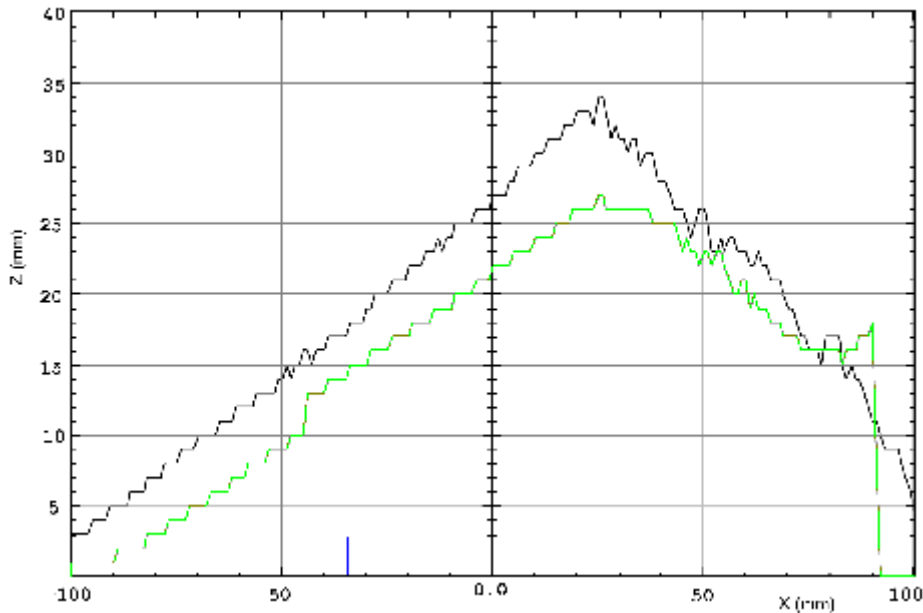


Figure 4.25: The dynamic aperture with 8 wigglers (in black) of $B=3.5\text{T}$ and $L=1.44\text{m}$, after tune compensation, compared to the original one (green).

The Cases of Less than 8 Wigglers of the Same Type: Although insertion of even number of wigglers is preferable because of their symmetric optical effects and less destruction for the dynamic aperture than that in case of odd number, nevertheless compensation procedure works well for any number of wigglers.

In these cases, in addition to the vertical tune shift there was a vertical beta beating.

The compensation scheme was *local* and it was simply done by changing the gradient in the two BMs near to each wiggler from each side and in the rest of the ring BMs independently. This means that the surface coils (which vary the gradient) in BMs should be divided into two families; that in the BMs near to the ID from each side in one family and the others in another family.

The compensation can be done *locally* for the beta beating, then *globally* for the tune shift or locally for all of them simultaneously. The maximum gradient variation needed for the compensation was 0.853% in case of 2 wigglers (with $B=3.5T$) and 1.3% in case of 4 wigglers. As an example, figures (4.26) and (4.27) show the optics with 2 and 3 wigglers, respectively, after the total compensation.

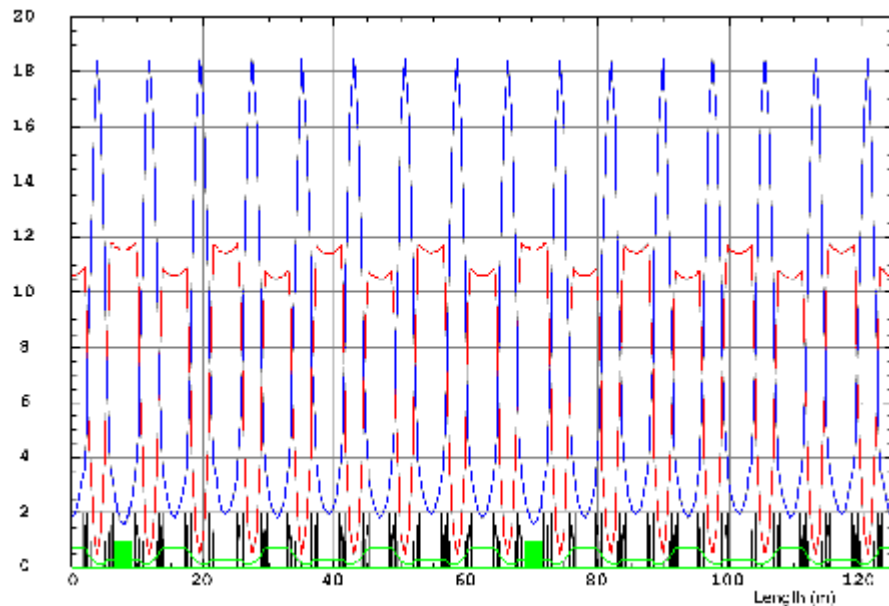


Figure 4.26: The optics with 2 wigglers of $B=2.5T$ and $L=2.4m$ after compensation.

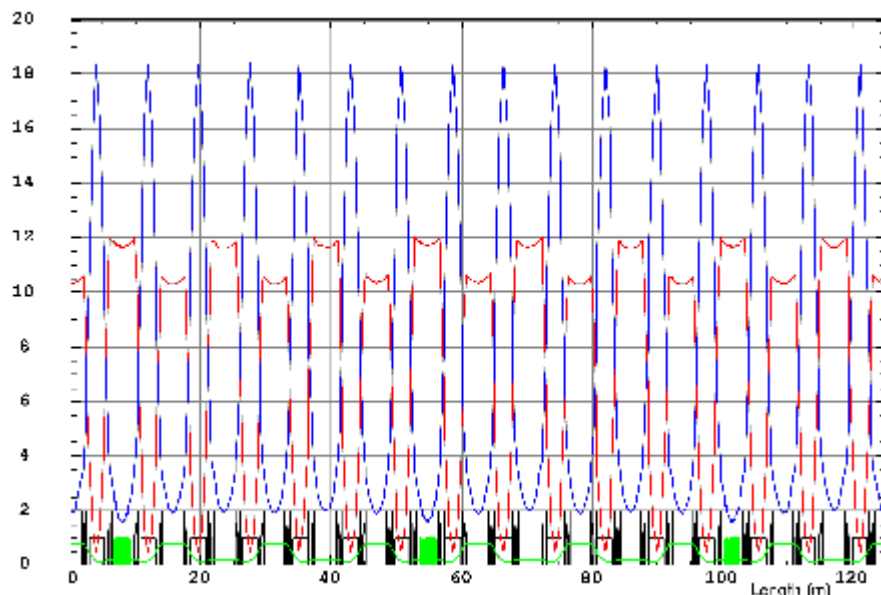


Figure 4.27: The optics with 3 wigglers of $B= 2.5T$ and $L= 2.4m$ after compensation.

To have an idea about the optical changes after compensation, the percentage optical difference between the optics before wigglers and the compensated one after wigglers has been calculated. This is shown in figure (4.28) for the case of 2 wigglers.

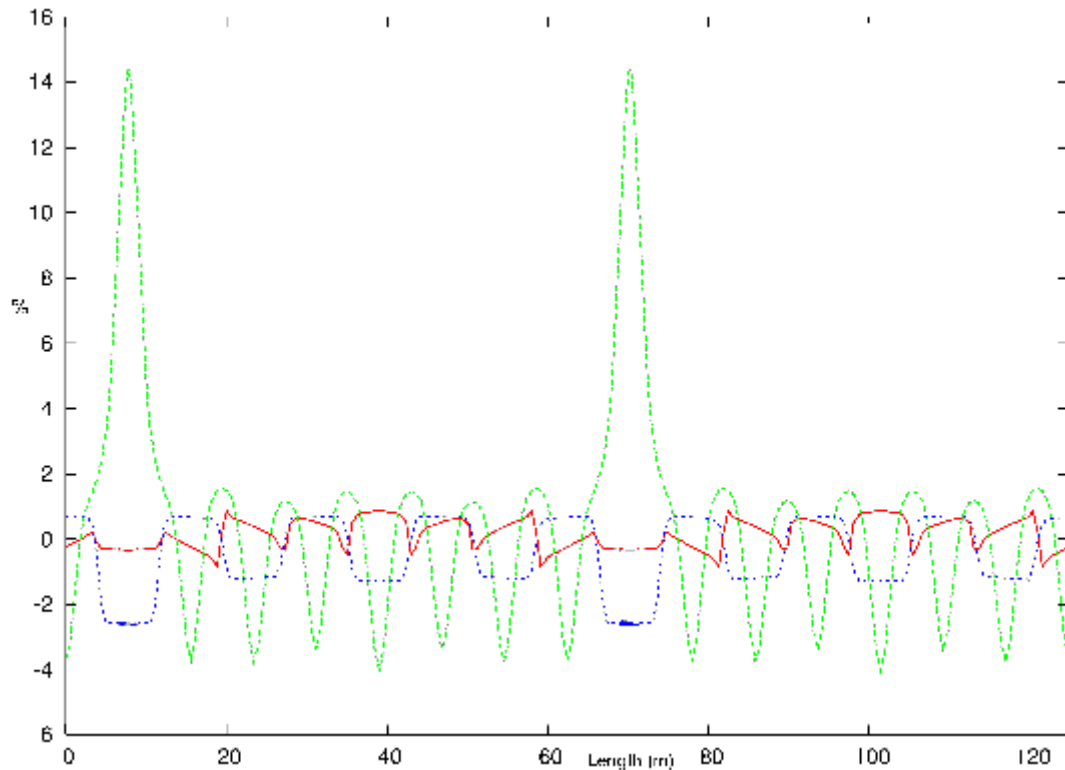


Figure 4.28: The optical difference [(original function – compensated function) / original] * 100% . The difference in β_x , β_z and dispersion appears in red, green and blue respectively. The maximum difference in β_z and dispersion are at the wigglers positions.

It can be seen from this figure that the largest optical difference is in β_z and at the wiggler position where it becomes about 14.5% (i.e. β_z in the new compensated optics with wigglers is 14.5% less than the original optics without wigglers) while it doesn't exceed 4% anywhere in the ring. The changes are smaller in β_x (<1%) and dispersion (<3% at the wiggler position).

These changes are negligible except that in β_z at wiggler position which is still not significant.

The dynamic apertures were reduced in both cases, but in case of 2 wigglers (figure 4.26) it is still larger than the needed physical aperture as shown in figure (4.29). However they can be enhanced by non linear optimisation.

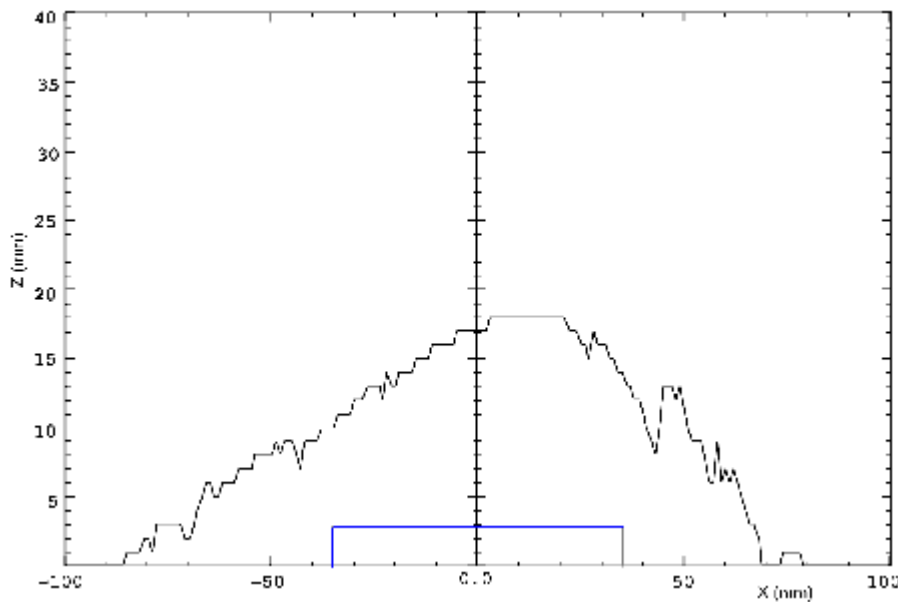


Figure 4.29: The dynamic aperture with 2 wigglers of $B = 2.5\text{T}$ and $L = 2.4\text{m}$ after total compensation.

The case of wigglers of different types: The possibility of using different wigglers with different characteristics called for testing the flexibility of the lattice in treating their effects.

As an example, 2 different wigglers of the above types were inserted in the lattice and the compensation for the resulted beta beating and tune shift has been done easily.

The compensation has been done *locally* by dividing the gradient in BMs into 3 families; each wiggler of different type was between two BMs containing one gradient family and the rest of the ring BMs contained gradients in one family. The maximum gradient variation needed for compensation was 0.9%. The optics after compensation is shown in figure (4.30).

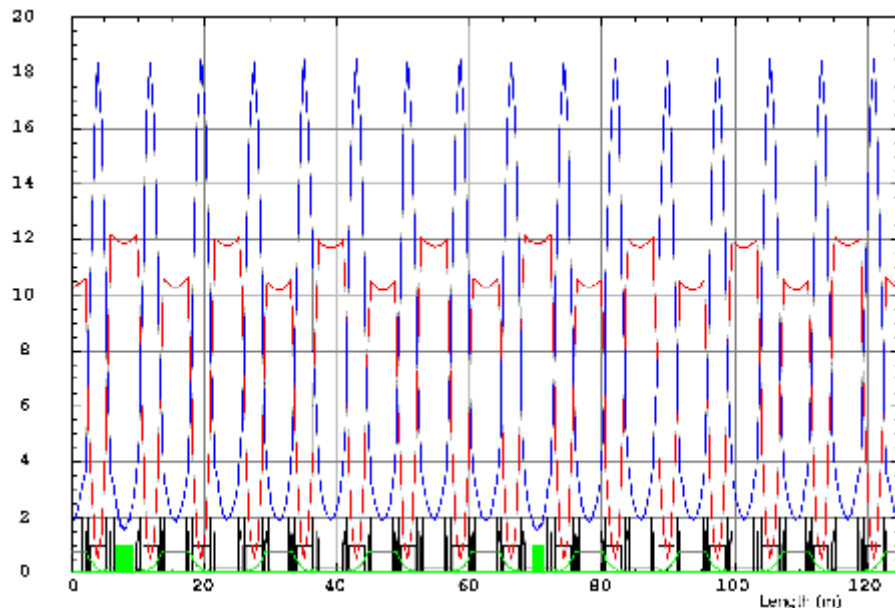


Figure 4.30: The optics, after total compensation, with 2 different wigglers: one of $B = 2.5\text{T}$, $L = 2.4\text{m}$ and the other of $B = 3.5\text{T}$, $L = 1.44\text{m}$.

All the compensation above has been done by varying the gradients by hand not by fitting, since it was not possible in the used code to put the gradient in the BM as a variable participating in fitting process.

The simplicity in dealing with SESAME lattice and the easiness in the compensation processes reflected a side of its flexibility and showed that the rigidity of the lattice had no significant impact on its performance.

4.4 Closed Orbit Distortion and Correction

Real machines contain different types of errors produced by misalignment of ring devices, magnetic field errors and several external error sources, which can be averaged statistically.

These errors cause distortion and instability for the beam closed orbit, which consumes the physical aperture, reduces the dynamic aperture, changes the optics and, in case of variation with time, it disturbs emittance and brilliance. So it must be corrected.

Closed orbit correction can be done by using corrector magnets and beam position monitors (BPMs).

Closed orbit distortion is caused mainly by dipolar kicks produced by some residual errors, mainly: misalignments of dipoles, field errors in dipoles and displacement of quadrupoles.

Because of the higher field gradient in the BMs together with high β_z there, a bit larger vertical closed orbit distortion, than in the first conceptual design, is expected for the same standard error types and values. Therefore a special care should be taken in aligning the BMs during installation as well as in their manufacturing to keep the field errors as small as possible.

To maintain the high brilliance of the radiation coming from the IDs and to minimize the unwanted closed orbit changes introduced by the wigglers, the closed orbit must be well corrected at the position of the wiggler. A deeper study for this issue will be done later.

By introducing 3 r.m.s values of the errors displayed by Table (4.7), the expected closed orbit distortion is calculated by real tracking of the particles over 100 different samples (i.e. 100 different tracking related to different probable error configuration). The horizontal and vertical closed orbit distortions are shown in figures (4.31) and (4.32) respectively.

Table 4.7: The error types introduced to the lattice.

Magnet type	Type of error	RMS value of error
Dipole	Field error	$5 \cdot 10^{-4}$
	Displacement $dx = dz = ds$	0.2 mm
	Rotation around s ($d\varphi_s$)	0.2 mrad
Quadrupole	Displacement $dx = dz$	0.1 mm

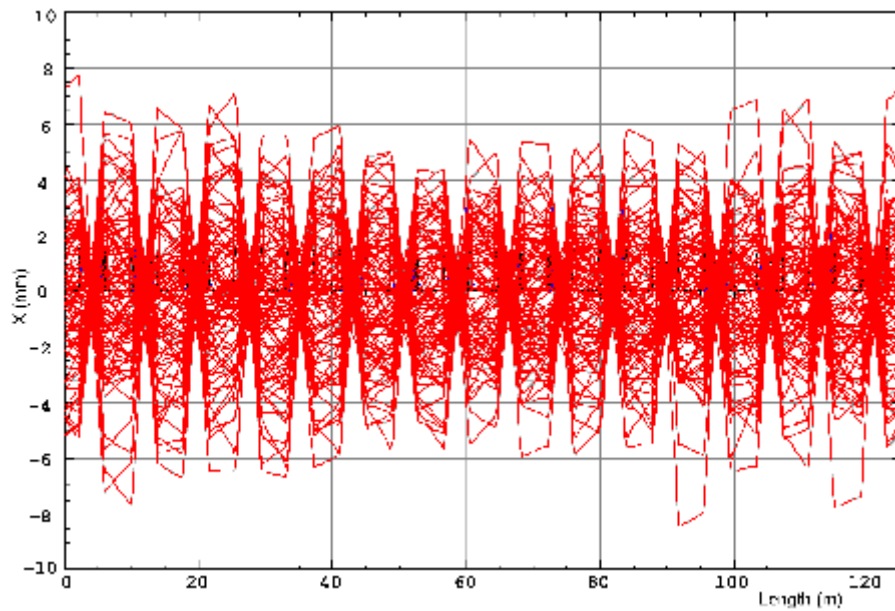


Figure 4.31: The uncorrected horizontal closed orbit distortion. The total ring is used.

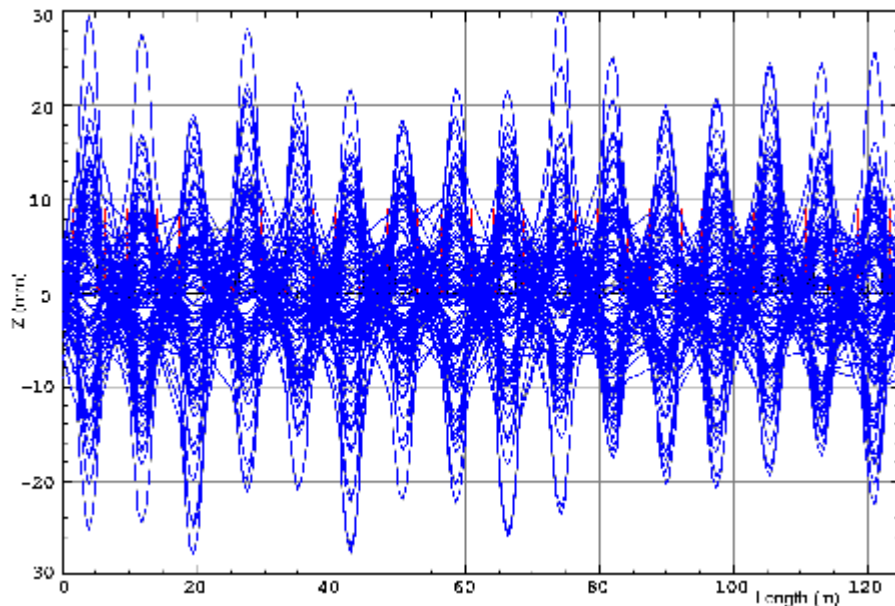


Figure 4.32: The uncorrected vertical closed orbit distortion.

Using 32 beam position monitors (BPMs), 32 horizontal and 32 vertical correctors placed in the sextupoles, the distorted closed orbit can be corrected to 1r.m.s residual distortion of 6 μm vertically and 33 μm horizontally in the ID straight section, while it is of 25 μm vertically and 40 μm horizontally in the BMs. This will be shown by figure (4.33).

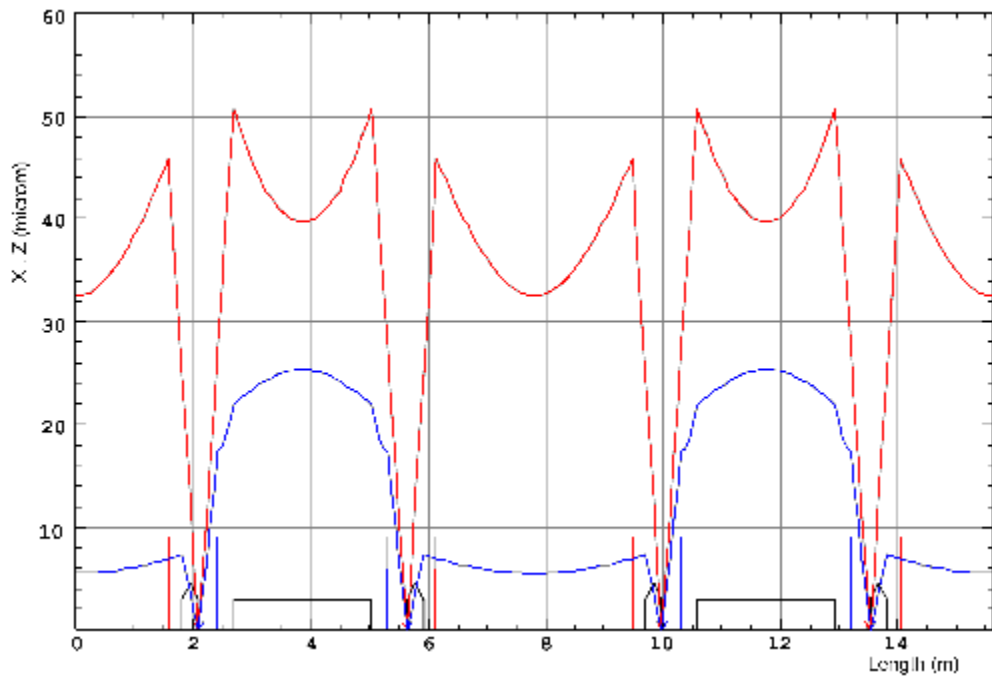


Figure 4.33: The corrected horizontal (in red) and vertical (in blue) closed orbit distortion using analytical statistical calculations.

A 3 r.m.s residual closed orbit distortion, calculated by a real particle tracking using 100 samples, is shown in figures (4.34) and (4.35).

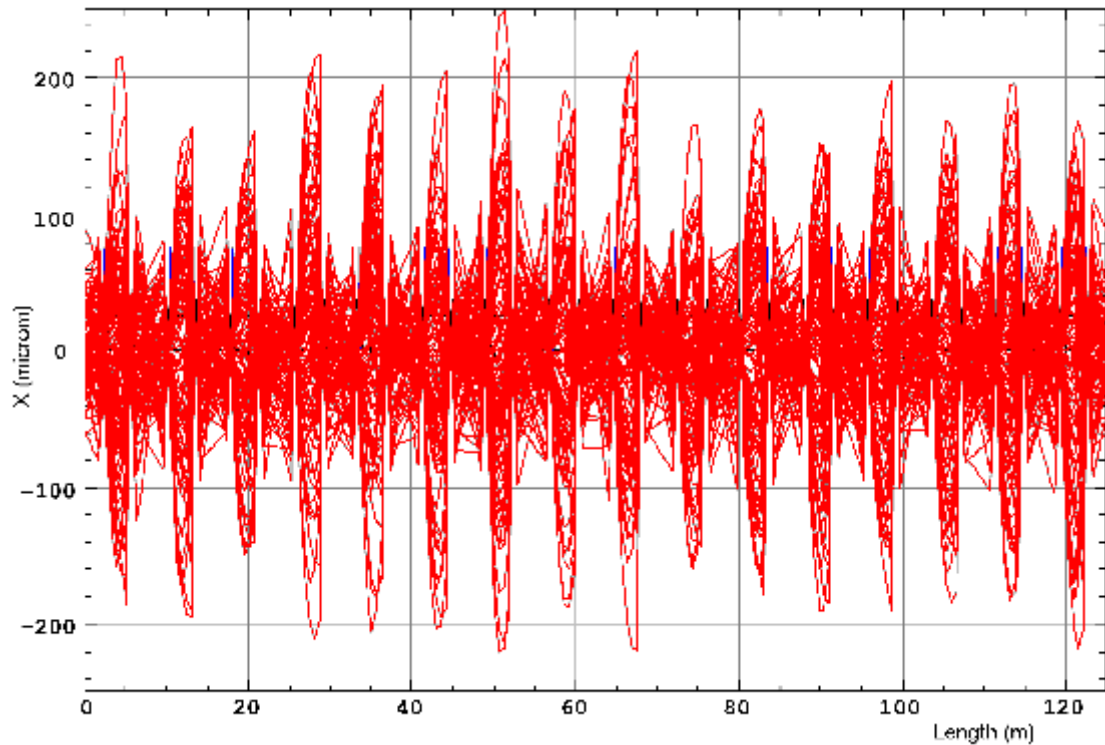


Figure 4.34: The corrected horizontal closed orbit distortion using tracking over 100 samples.

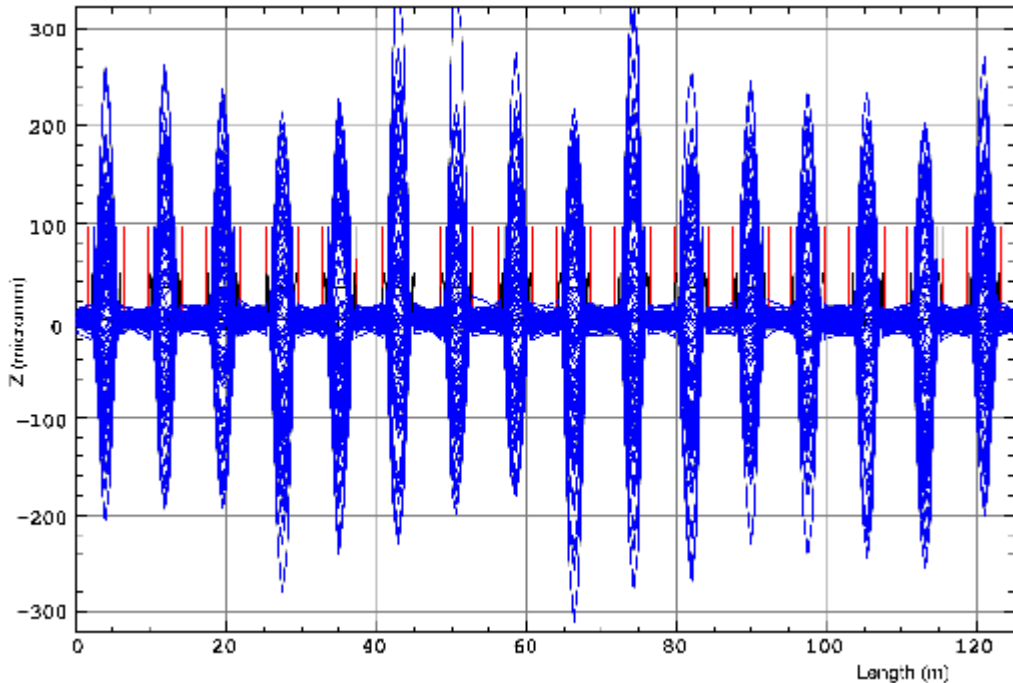


Figure 4.35: The corrected vertical closed orbit distortion using tracking over 100 samples.

4.5 The Coupling

The coupling between the vertical and horizontal emittance is determined by the misalignment of the magnets in the horizontal or vertical plane. Due to these errors, the horizontal betatron oscillations and dispersion will be transformed partially to the vertical plane, which leads to a creation of the vertical emittance. The value of this transformation depends on the coupling which is represented by the coupling factor κ as can be seen from equations (4.9):

$$\begin{aligned}\varepsilon_z &= \kappa \varepsilon_x \\ \varepsilon_x &= \varepsilon_0 / (1 + \kappa) \\ \varepsilon_z &= \kappa \varepsilon_0 / (1 + \kappa)\end{aligned}\tag{4.9}$$

Where ε_z is the vertical emittance, ε_x is the horizontal emittance and ε_0 is the natural emittance.

With a perfect alignment the coupling would be zero and so the vertical emittance too.

The alignment of the magnets at SESAME will be made with the same precision as for other light sources too. Hence for SESAME we will have roughly also the same coupling factor.

After the errors of table (4.7), in addition to a quadrupole rotation of .2 mrad around the longitudinal s axis, have been introduced to SESAME lattice and the closed orbit distortion has been corrected, the average coupling in the ring was $\kappa = 3.5 \cdot 10^{-3}$. This has been done by tracking the particle over 100 different samples.

4.6 Specifications of the Magnets

Due to the change in the machine energy, the magnetic parameters were changed in order to get the required optics and to keep compatible with the recent changes. The specifications of the magnetic elements for the original optics shown in figure (4.2) will be given in the following subsections. Some of these parameter may change a little bit due to the different optical optimisations to be done to accommodate the IDs.

4.6.1 The Bending Magnets

All these elements in the storage ring have the same parameters, so they are in one family. However the gradient can be changed by small percentages in some of them depending on the compensation scheme used to compensate for the unwanted optical effects of the IDs. This gradient variation can be done by independent surface coils which means that these coils can be divided into more than one family.

The original parameters common to all the BMs in the ring are displayed by table (4.8):

Table 4.8: Magnetic parameters of the BMs.

Parameter	Unit	Value
Magnetic Length	m	2.34
Bending angle	radian	0.3927
Bending radius	m	5.9565
Magnetic field gradient	T/m	-3.032

4.6.2 The Quadrupole Magnets

These elements are divided into 2 horizontally focusing families. Their parameters are shown in table (4.9):

Table 4.9: Magnetic parameters of the quadrupoles.

Family	Q1	Q2
Magnetic Length (m)	0.265	0.265
Magnetic field gradient (T/m)	17	16.92

4.6.3 The Sextupole Magnets

These elements are divided into 4 families, each family has the same parameters as shown in table (4.10). The sextupole strength (m) is defined by $m(m^{-3}) = (1/2B\rho)\partial^2Bz/\partial x^2$.

Table 4.10: Magnetic parameters of the sextupoles.

Family	S1	S2	S3	S4
Magnetic Length (m)	0.14	0.14	0.14	0.14
Magnetic Strength (m^{-3})	9.194	-12.92	-12.6	8.947

4.6.4 The Corrector Magnets

These elements will be as coils inside the sextupoles having the same length of the sextupoles. There will be two types of correctors to correct the closed orbit: horizontal and vertical ones to correct the horizontal and vertical closed orbit distortion, respectively. Table (4.11) shows their parameters.

Table 4.11: Magnetic parameters of the corrector magnets.

Type of Corrector	Horizontal	Vertical
Magnetic Length (m)	0.14	0.14
Maximum Kick (radian)	$1.115 \cdot 10^{-4}$	$7.113 \cdot 10^{-5}$

4.7 The Beam Lifetime

As mentioned in the previous white book, the lifetime of the electron beam is a composition of two major lifetimes; the gas scattering lifetime (τ_g) and Touschek lifetime (τ_{Tous}), where the total lifetime is:

$$1/\tau = 1/\tau_g + 1/\tau_{\text{Tous}} \quad (4.10)$$

4.7.1 The Gas Scattering Lifetime

This lifetime is determined by the scattering process of the beam electrons by the residual gas molecules inside the vacuum chamber which makes it strongly inversely-dependent on the pressure inside the vacuum chamber. The ability to reach a low vacuum pressure will increase this lifetime.

The scattering process can happen by two mechanisms:

Elastic Scattering (Coulomb Scattering): In which the beam electron is deflected elastically (without energy loss) either by the nuclei or the shelf electrons of the heavy gas molecules resulting in increasing the betatron amplitudes of the deflected electron. An enough high betatron amplitudes will cause the electron to be lost at the physical or dynamic aperture limits.

Inelastic Scattering: In this case the electron is deflected inelastically and suffers from energy loss either by emitting photons (Bremsstrahlung) or by transferring that energy to the molecules. The second case has a very small cross section, so it will not be considered. The energy loss may cause the electron to go out of the RF energy acceptance. In non-zero dispersion sections the scattered electron will oscillate around another closed orbit (off-momentum closed orbit), which increases the total betatron amplitudes. This may cause the electron to be lost at the transverse (physical or dynamic) aperture. An enough energy loss will cause the electron to be lost at the minimum [RF acceptance, physical acceptance, dynamic acceptance].

4.7.1.1 Elastic Nucleus-Scattering Lifetime (τ_{coul}):

The dependence of this lifetime on the square of the machine energy will increase it from the first white book lattice case. But the presence of in-vacuum undulator has minimised the vertical physical acceptance which had a decreasing effect on the τ_c due to their direct proportionality.

The minimum vertical half-aperture will be, at the in-vacuum undulator, of 3mm. This made the minimum vertical acceptance to be there:

- $(A_z^2 / \beta_z) = (0.003)^2 / 1.73 = 5.2 \cdot 10^{-6} \text{ m.rad.}$

The minimum horizontal physical acceptance is always at the septum position if it was at $x < 34.6$ mm from the axis of the vacuum chamber. On the condition that the septum will be at $x = 27.5$ mm, the horizontal acceptance will be:

- $(A_x^2 / \beta_x) = (0.0275)^2 / 10.9 = 6.94 \cdot 10^{-5} \text{ m.rad.}$

With $\langle \beta_x \rangle = 7.54$ m and $\langle \beta_z \rangle = 7.45$ m in the storage ring, the nucleus-Coulom scattering at $P = 2 \text{ nTorr}$ will be:

$$\tau_{\text{Coul}} = 46 \text{ hours}$$

While at $P = 1 \text{ nTorr}$, it will be:

$$\tau_{\text{Coul}} = 92.1 \text{ hours}$$

4.7.1.2 Elastic Shelf Electron-Scattering Lifetime ($\tau_{\text{coul}}(e)$):

This lifetime is directly proportional to the machine energy and the minimum energy acceptance. Increasing the machine energy to 2.5 GeV will increase this lifetime from the last version case. The machine energy acceptance will be limited by the RF one at the beginning.

With the RF acceptance of 1.3 %, this lifetime at $P = 2 \text{ nTorr}$ will be:

$$\tau_{\text{Coul}}(e) = 1317.8 \text{ hours}$$

While at $P = 1 \text{ nTorr}$, it will be:

$$\tau_{\text{Coul}}(e) = 2635.6 \text{ hours}$$

Due to its length, the effect of this lifetime on limiting the total beam lifetime will be negligible so far.

4.7.1.3 Inelastic Nucleus-Scattering Lifetime (τ_{brem}):

The cross section of this process is large which has its noticed effect on limiting the total beam lifetime.

This lifetime is proportional to the minimum energy acceptance which will be the RF one at the beginning.

With the RF acceptance of 1.3%, at $P= 2 \text{ nTorr}$ the lifetime will be:

$$\tau_{\text{Brem}} = 28.17 \text{ hours}$$

While at $P= 1 \text{ nTorr}$, it will be:

$$\tau_{\text{Brem}} = 56.34 \text{ hours}$$

4.7.1.4 Inelastic Shelf Electron-Scattering Lifetime ($\tau_{\text{brem}}(e)$):

It is indirectly affected by the machine energy and the minimum energy acceptance.

With the RF energy acceptance of 1.3% and at $P= 2 \text{ nTorr}$, it will be:

$$\tau_{\text{Brem}}(e) = 65.4 \text{ hours}$$

While at $P= 1 \text{ nTorr}$, it will be:

$$\tau_{\text{Brem}}(e) = 130.8 \text{ hours}$$

4.7.1.5 The Total Gas Scattering Lifetime

So, the total gas scattering lifetime (τ_g) is calculated as the following:

$$1/\tau_g = 1/\tau_{\text{Coul}}(e) + 1/\tau_{\text{Brem}}(e) + 1/\tau_{\text{Brem}}(e) \quad (4.11)$$

Which means that τ_g at $P=2 \text{ nTorr}$ will be:

$$\tau_g = 13.64 \text{ hours}$$

While at $P= 1 \text{ nTorr}$, it will be:

$$\tau_g = 27.29 \text{ hours}$$

4.7.2 Touschek Scattering Lifetime

The Touschek scattering process happens inside the electron beam itself, independently from the pressure in the vacuum chamber. The collision between the electrons in the beam cause momentums transfer between them which results in electron momentum deviations either by loss or gain momentum. If the momentum deviation exceeded the RF momentum acceptance limit, the particle almost will be lost. On the other hand, in non-zero dispersion sections, the off-momentum particle will oscillate around different closed orbit which will increase the total betatron oscillation amplitude. In case of enough high oscillations, the particle will be lost either at the physical or the dynamic aperture limit. In general, for an enough off-momentum deviation the particle will be lost at the minimum [RF acceptance, physical acceptance, dynamic acceptance].

This process is the dominant one in the storage ring and has the most significant effect in limiting the beam lifetime.

As Touschek lifetime depends on the 3rd power of machine energy, this will participate in its increase from the 2 GeV case.

Because of the Touschek lifetime dependence on the electron density in the bunch, the value of the ‘beam current /bunch’ and the volume of the bunch have principal effect on it.

Although the septum position will minimise the chamber energy acceptance, the machine acceptance at the beginning will be limited by the RF one (1.3%).

The Touschek lifetime will be calculated for the following constant conditions:

- The maximum momentum deviation $\Delta P/P = \pm 3\%$
- The RF energy acceptance = 1.3%
- The coupling = 1%
- The natural bunch length = $4.2157 \cdot 10^{-11}$ s
- The vacuum chamber half-dimensions is 15 mm in vertical except 3mm at the in-vacuum undulator and 35 mm in horizontal except 27.5 mm at the septum.

Since it will be useful to know the beam lifetime at different current values, Touschek lifetime will be calculated for different beam average current values: 100, 200, 300 and 400 mA. On the condition that a 70% of the storage ring will be filled with current, the current/bunch (I_b) will be:

- $I_b = 0.6875, 1.375, 2.0625$ and 2.75 mA respectively.

According to the above conditions, Touschek lifetime τ_{Tous} was as given in table (4.12):

Table 4.12: Touschek lifetime at different beam current values.

Beam current (mA)	100	200	300	400
τ_{Tous} (hour)	241.9	120.95	80.65	60.45

It should be noted that the effect of I_b value on the bunch length was not taken into account.

4.7.3 The Total Beam Lifetime

In order to calculate the total beam lifetime at different beam current values, the pressure has been calculated at these different values at 100 Ah beam dose. This will make the gas scattering lifetime changeable with the beam current value. Using the above Touschek lifetime calculations, the total beam lifetime τ has been calculated to be as shown in table (4.13).

In the sake of comparison, the total beam lifetime has been calculated also at machine energy of 2 GeV for the same above conditions taking into account the change in the RF energy acceptance which becomes 0.967%, and the change in the natural bunch length which becomes $4.532 \cdot 10^{-11}$ s, on the condition that the over voltage factor keeps 3.36. This is shown also in table (4.13).

Table 4.13: The gas scattering, Touschek and total lifetimes at different beam currents and machine energies.

Beam average current (mA)	Machine Energy = 2.5 GeV				Machine Energy = 2 GeV			
	Pressure (nTorr)	τ_g	τ_{Tous}	τ	Pressure (nTorr)	τ_g	τ_{Tous}	τ
100	.542	50.35	241.9	41.67	0.51	43.5	38.62	20.5
200	.812	33.61	120.95	26.3	0.74	30	19.3	11.74
300	1.083	25.2	80.65	19.2	0.98	22.64	12.87	8.2
400	1.354	20.15	60.45	15.1	1.2	18.49	9.65	6.34

The desire to get a good beam lifetime needs a special care about the vacuum system and the vacuum chamber treatment.

References

- [1] The first white book and its references.